AD-A094 197 GEORGE WASHINGTON UNIV WASHINGTON D C SCHOOL OF ENGI--ETC F/G 11/6
FATIGUE AND MICROSTRUCTURAL PROPERTIES OF QUENCHED TI-6AL-4V, A--ETC(U)
SEP 80 C M GILMORE, M A IMAM, M SUGANO N00019-78-C-0269
UNCLASSIFIED TR-5 NL

1 of 2
AD A094197

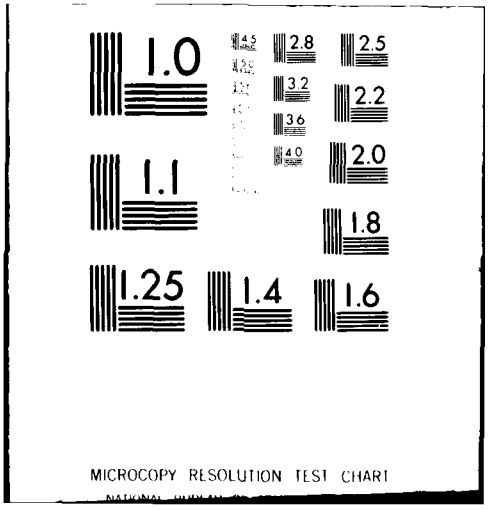
1.0
1.1
1.25
1.4
1.6
1.8
2.0
2.2
2.5
2.8
3.2
3.6
4.0
MICROCOPY RESOLUTION TEST CHART

LEVEL b

(5)

AD A094197

THE GEORGE WASHINGTON UNIVERSITY

STUDENTS FACULTY STUDY R ESEARCH DEVELOPMENT FUT URE CAREER CREATIVITY CC MMUNITY LEADERSHIP TECH NOLOGY FRONTIE ESIGN ENGINEERING APP ENC GEORGE WASHIN NIV

SCHOOL OF ENGINEERING AND APPLIED SCIENCE

8

A. FATIGUE AND MICROSTRUCTURAL PROPERTIES OF QUENCHED Ti-6Al-4V,

B. A CRYSTALLOGRAPHIC STUDY OF FATIGUE DAMAGE IN TITANIUM,

C. CORROSION AND CORROSION-FATIGUE BEHAVIOR OF Ti-4.5Al-5Mo-1.5Cr (CORONA 5) AND Ti-6Al-4V.

by

C. M. Gilmore, M. A. Imam and M. Sugano

Final Report,
September 1980

Prepared Under Contract N00019-78-C-0269

For The

NAVAL AIR SYSTEMS COMMAND
Washington, D.C. 20361

Approved For Public Release
Distribution Unlimited

Technical Report No.
V

FATIGUE AND MICROSTRUCTURAL PROPERTIES OF QUENCHED Ti-6Al-4V

M. A. Imam and C. M. Gilmore*

ABSTRACT

The mechanical properties and microstructures of Ti-6Al-4V were determined for specimens heat treated at temperatures from 845°C to 1065°C for 10 minutes and water quenched; these properties were compared with those of α-β annealed specimens. Specimens heat treated at 900°C and water quenched had higher fatigue lives by a factor of four to ten relative to the other treatments, in addition this treatment resulted in high ductility, yield strength, tensile strength and elastic modulus. Microstructure studies utilizing optical and transmission microscopy showed that the improved fatigue lives were a result of a strain induced transformation of retained β to α′ martensite. Isothermal aging of as quenched specimens reduced the fatigue lives and the retained β was thermally activated to transform to α′ martensite. The β to α′ martensite transformation observed was therefore an isothermal martensite transformation whereas it is presently assumed that this transformation is always athermal. The amount of retained β and its relative stability was shown to depend upon the heat treatment temperature.

M. A. Imam and C. M. Gilmore are respectively Research Scientist and Associate Professor, The School of Engineering and Applied Science, The George Washington University, Washington, D.C. 20052. This work was submitted in partial fulfillment of the degree of Doctor of Science by M. A. I.

The lower the heat treatment temperature below the β transus the smaller the amount of β phase present before the quench and the richer the β phase in β stabilizer. The greater the concentration of β stabilizer in the β phase the greater the probability that the β phase was retained. Low heat treatment temperatures resulted in a small amount of more stable β phase, and high heat treatment temperatures resulted in a greater amount of β that was less stable and was more probable to transform to α´ martensite during a water quench.

LIST OF TABLES

Table I. Fatigue Lives of Thermally Treated Ti-6Aℓ-4V Alloys Cycled at a Shear Strain of ± 0.02 at 0.2 Hz

Table II. Fatigue Lives of Heat Treated (900°C) and Aged (500°C and 760°C) Ti-6Aℓ-4V Alloys Cycled at a Shear Strain of ± 0.02, a Frequency of 0.2 Hz

Table III. Fatigue Lives for Tension-Compression Tests with σ_{max} = 827 MPa (120 ksi), R = -0.3

Table IV. Tensile Test Results for Ti-6Aℓ-4V

Table V. Microhardness of Thermally Treated Ti-6Aℓ-4V Alloys

Table VI. Microchemistry of Thermally Treated Ti-6Aℓ-4V Alloys

Table VII. Lattice Parameters of Ti-6Aℓ-4V Phases

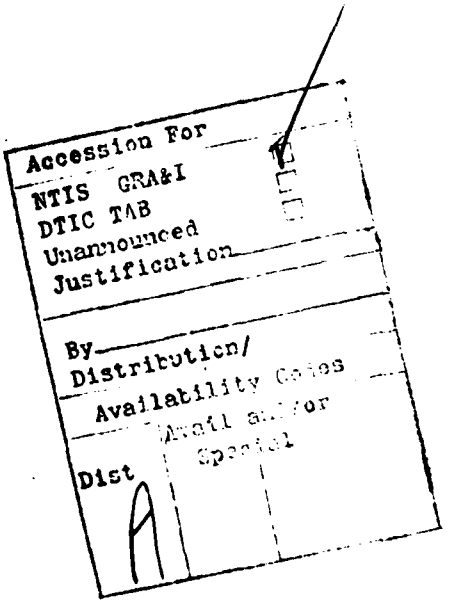

LIST OF FIGURE CAPTIONS

Figure 1. Torsion Fatigue Specimen Design

Figure 2. The Machine for Torsional Fatigue

Figure 3. Tension-compression Fatigue Specimen Design

Figure 4. Cycles to Failure as a Function of the Applied Alternating Shear Strain for Specimens α-β Annealed, and Heat Treated at 900°C and Water Quenched

Figure 5. Transmission Electron Micrograph of α-β Annealed Microstructure Showing Grain Boundary β-Ti (Arrow) along with α-Ti Grains

Figure 6. Optical Micrograph of Ti-6Aℓ-4V Heat Treated at 843°C (1550°F) and Water Quenched Showing α-Ti (Labeled x) and β-Ti

Figure 7. Transmission Electron Micrograph of Ti-6Aℓ-4V Heat Treated at 843°C (1550°F) and Water Quenched Showing α-Ti (Labeled x) and β-Ti

Figure 8. Optical Micrograph of Ti-6Aℓ-4V Heat Treated at 900°C (1650°F) and Water Quenched Showing α-Ti (Labeled x) and β-Ti. The β-Ti Phase Contains α′-Ti Martensite Which is Not Visible Here

Figure 9. Transmission Electron Micrograph of Ti-6Aℓ-4V Heat Treated at 900°C (1650°F) and Water Quenched. The Diffraction Pattern was Taken from the Area of the Alloy that Indexes as a Mixture of α′-Ti Martensite and β-Ti

Figure 10. Transmission Electron Micrograph (Dark Field) of Ti-6Aℓ-4V Heat Treated at 900°C (1650°F) and Water Quenched Showing the Morphology of Martensite. Dark Field Reflection is the α′-Ti (0111)

Figure 11. Optical Micrograph of Ti-6Aℓ-4V Heat Treated at 900°C and Water Quenched Followed by Aging at 500°C for One Hour

Figure 12. Transmission Electron Micrograph of Ti-6Aℓ-4V Heat Treated at 900°C and Water Quenched Followed by Aging at 500°C for One Hour Showing α-Ti and the Phase Region where α′-Ti Martensite has Grown

Figure 13. Optical Micrograph of Ti-6Aℓ-4V Heat Treated at 900°C (1650°F) and Water Quenched Followed by Aging at 500°C for 8 Hours

Figure 14. Transmission Electron Micrograph of the Same Specimen as in Figure 13 Showing α-Ti (Labeled x) and the phase Region where α′-Ti Martensite Has Grown

Figure 15. Optical Micrograph of Ti-6Aℓ-4V Heat Treated at 900°C (1650°F) and Water Quenched Followed by Aging at 760°C (1400°F) for One Hour

Figure 16. Transmission Electron Micrograph of the Same Specimen as in Figure 15 Showing α-Ti and Grain Boundary β-Ti

Figure 17. Transmission Electron Micrograph of the Same Specimen as in Figure 9 Taken Close to the Fracture Surface after Tension-compression Fatigue Failure Showing Sharp Needles of α′-Ti Martensite and α-Ti Grains

Figure 18. Optical Micrograph of Ti-6Aℓ-4V Heat Treated at 927°C (1700°F) and Water Quenched Showing α-Ti and β-Ti. The β-Ti Phase Contains α′-Ti Martensite

Figure 19. Transmission Electron Micrograph of the Same Specimen as in Figure 18, Showing α-Ti and the Phase Region β-Ti and α′-Ti Martensite

Figure 20. Optical Micrograph of Ti-6Aℓ-4V Heat Treated at 954°C (1750°F) and Water Quenched Showing α′-Ti Martensite

Figure 21. Optical Micrograph of Ti-6Aℓ-4V Solution Treated at 1065°C (1950°F) and Water Quenched Showing α′-Ti Martensite

Figure 22. Transmission Electron Micrograph of the Same Specimen as in Figure 21. The Electron Diffraction Pattern Indexes to be α′ (Hexagonal) Martensite

Figure 23. Microchemistry of Ti-6Aℓ-4V Alloy as a Function of Quenching Temperature. The Hold Time at Temperature was 10 Minutes

INTRODUCTION

Titanium alloys such as the Ti-6Aℓ-4V can have numerous microstructures and it has been demonstrated that the microstructure of titanium alloys can have a significant effect on fatigue properties [1-14]. In the alloy Ti-6Aℓ-4V, the vanadium stabilizes the β (BCC) phase of titanium and the aluminum stabilizes the α (HCP) phase so that at low temperatures it is possible to have in equilibrium a vanadium rich β phase and an aluminum rich α phase. At temperatures above the β transus titanium alloys are entirely of the β phase. Rapid cooling of the β phase from above the β transus results in the formation of a hexagonal close packed martensitic phase α′. One of the earliest review papers that discusses these phase transformation is by Jaffee [15].

Solution treated and quenched carbon steels are generally brittle immediately after a quench because the iron-carbon martensite is quite brittle and tempering of the steel is necessary. Thus, metallurgists generally avoid the as quenched metallurgical condition; however, there are some observations in the literature that indicate as quenched microstructures of titanium alloys might have some interesting properties. Stubbington and Ballett have observed that fatigue failure of electron beam welded Ti-6Aℓ-4V occurred in the base metal and not in the weld [16]. Electron beam welds are rapidly cooled

in a way similar to quenching. Crossley and Lewis observed that solution treatment at 1065°C (1950°F) and water quenching of Ti-6Aℓ-4V resulted in slower crack propagation than in equiaxed α-β microstructures[17]. Sherman and Kessler observed that solution treating at 843°C (1550°F) and water quenching resulted in a metal alloy with low yield strength, good machinability and excellent low temperature formability[18]. Thus, it is obvious that solution treatment and water quenching of the alloy Ti-6Aℓ-4V does not necessarily produce a brittle metal, and it may be possible that some useful properties might result from solution treated and quenched titanium alloys, however, very little work has been conducted on as quenched titanium alloys.

The phase transformations, microstructures, and physical properties of the alloy Ti-6Aℓ-4V have been investigated by several authors. One of the studies of solution treated Ti-6Aℓ-4V was conducted by Fopiano et al.[19]. It was observed that the β phase when water quenched from solution temperatures of 800°C (1472°F) or higher always formed the α′ phase. Thus, Ti-6Aℓ-4V solution treated at temperatures below the β transus (approximately 1000°C) and water quenched should always form a mixture of primary α that existed before the water quench and α′ formed by martensitic transformation of the high temperature β phase. They also observed that solution treating at 750°C (1382°F) resulted in primary α and β; the β phase appeared to be stable during water quenching from 750°C (1382°F). An in-

teresting observation by Fopiano was that increasing solution treatment temperatures from 850°C to 950°C produced a significant increase in hardness without any significant decrease in ductility. The observation of an increase in hardness without a decrease in ductility in an alloy system appeared to be due to a strengthening mechanism that might offer the opportunity of producing a material with good fatigue life. In this work we utilized heat treatments similar to Fopiano's and we determined the resulting effect upon fatigue life, tensile properties, hardness and microstructure. Properties were then analyzed in relation to the alloy microstructures.

The terminology heat treatment was utilized in this work when the specimen was held at a temperature below the β transus, and the terminology solution treatment was utilized only for temperatures above β transus that result in one solid solution. Hold temperatures below the β transus result in segregation into two phases.

EXPERIMENTAL PROCEDURES

In the tests that were conducted two different sizes of the alloy of slightly different compositions were utilized. This was necessary because tensile tests and tensile fatigue tests required 3.18 cm (1.25 inch) diameter bar stock. However, most of the fatigue tests were conducted in cyclic torsion which required 0.64 cm (0.25 inch) diameter rod. The 0.64 cm alloy is noted as Alloy Number 1 in the text and the 3.18 cm material is noted as Alloy Number 2.

Alloy 1: The alloy Ti-6Aℓ-4V was purchased from Alloy Specialities Incorporated, Garden Grove, California (Heat No. 600234-5357) as extruded 0.64 cm diameter rod with a composition in weight percent:

Aℓ	V	O	Fe	N	C	H
6.4	4.0	0.141	0.18	0.014	0.01	55 ppm

The alloy was mill annealed in vacuum for 2 hours at 704°C (1300°F) and air cooled. The β transus of this alloy was listed by the manufacturer as 985°C± 14°C (1805°F± 25°F)

Alloy 2: The alloy Ti-6Aℓ-4V was provided by the Naval Ship Research and Development Lab, Annapolis, MD (Heat No. 304171-06) as 3.18 cm extruded rod with a composition in weight percent:

Aℓ	V	O	Fe	N	C	H
6.3	4.2	0.188	0.17	0.01	0.02	67 ppm

The alloy was mill annealed, after extrusion for 2 hours at 704°C (1300°F).

Thermal Treatments

The thermal treatment or the solution treatment was performed in a vertical Centorr air furnace. Once the specified furnace temperature was attained, the specimens, attached to one end of a steel wire, were pulled into the heating zone of the furnace. A chromel alumel thermocouple was placed in the heating zone. After 10 minutes of thermal treatment at temperature, the suspended specimens were dropped directly from the furnace into a bucket containing water at room temperature. The temperature of the furnace was controlled to within ± 2°C. After quenching, the oxide affected surface layer of 0.05 cm (0.02 inch) was removed from the specimen surface. After quenching some specimens were aged at 500°C (932°F) and 760°C (1400°F) for times up to 8 hours. The equipment for aging was the same as for the annealing discussed below.

The α-β Anneal (αβA) alloy was annealed at 800°C (1472°F) for 3 hours, furnace cooled (FC) to 600°C (1112°F), and air cooled (AC) to room temperature. This annealing procedure was utilized as a standard for comparison with the other thermal treatments. A vacuum tube furnace was used for annealing and tempering. During annealing or aging, a pressure of 10^{-5} Torr or lower was maintained, and the furnace temperature was controlled to within ± 2°C. In the process of annealing, furnace cooling refers to cooling to the desired temperature with the furnace in place; air cooling means that the heater was pulled away from the vacuum tube with specimens inside.

Specimen blanks for constant strain amplitude fatigue tests were cut to 7.0 cm length from a 0.64 cm diameter extruded and mill annealed rod (Alloy No. 1). The specimen blanks were annealed or thermally treated according to the procedures listed above. The specimens were then machined and polished to the specimen dimensions shown in Figure 1 with the gage section polished to a 0.05 cm μM (alumina-powder) surface.

The constant strain amplitude fatigue tests were conducted with a facility shown in Figure 2. A fully reversed (R= -1) sinusoidal twist was applied to one end of the specimen. The other end of the specimen was fixed with respect to twisting motion, but it was free to move in the axial direction. A small constant axial stress of 21.2 Mpa was applied to the specimen through a weight and pully system to determine fatigue-cyclic creep interaction, but this will be treated in a separate publication. The tests were conducted with a frequency of 0.2 Hz.

Tension-compression constant stress amplitude fatigue tests were performed to provide a confirmation of results from constant shear strain amplitude tests. Specimen blanks for constant stress amplitude fatigue tests were cut to 20.32 cm length from a 3.18 cm diameter extruded and mill annealed rod (Alloy No. 2). The specimen blanks were machined to the approximate specimen dimensions shown in Figure 3. The specimens were then annealed or thermally treated according to the same procedures discussed above. After thermal treatment, at

least 0.05 cm of metal were machined and polished from the specimen to the final dimensions shown in Figure 3, with the reduced central section polished to a 0.05 μM (alumina powder) surface finish.

The constant stress amplitude fatigue tests were conducted on an MTS Series 810 system. In this investigation, a tension-compression mode with an R value of -0.3 was used. The maximum tensile stress was 758 MPa for a sinusoidal wave of 10 Hz frequency.

Specimens for the tensile tests were made from 3.18 cm diameter Ti-6Aℓ-4V rod (Alloy 2) according to the ASTM Specification E 8[20]. This specification suggests a diameter of 1.27 cm and a gage length of 5.08 cm. The MTS Series 810 System was used for the tensile tests. The load and strain were obtained from the load cell and extensometer, and the output was fed into an x-y recorder. Tensile tests were conducted on an α-β annealed microstructure and thermally treated specimens. Two specimens of each thermal treatment were tested.

Specimens for microhardness measurements were prepared by electropolishing in a solution of 55.4% methanol, 38% butanol and 6.6% of 70% perchloric acid at 14 volts and 0°C. Microhardness measurements were made with a Wilson Tukon Microhardness Tester using a Knoop indenter with a load of 100 grams. The measurements were repeated 8 times for each specimen.

Microstructural analyses were conducted using the methods of optical microscopy, scanning and transmission electron microscopy, and selected area electron diffraction. Unless otherwise

specified all microscopy work was conducted on Alloy No. 2.

Specimens for optical microscopic observations were mounted, mechanically polished to a 0.05 μM (alumina powder) surface finish, and etched with Kroll's etchant (3.5% HNO_3, 1.5% HF and 95% H_2O). The optical microscopy was done with a Carl Zeiss, Ultraphot II microscope or a Leitz Wetzlar microscope.

Specimens for scanning electron microscopy were electropolished as discussed above and after electropolishing, the surface was etched with Kroll's etchant. The scanning microscopy was done with a Cambridge 'Stereoscan' Scanning Electron Microscope, Type 96113, Mark 2A with excitation voltage of 20 Kv.

Thin foils for transmission electron microscopy and selected area electron diffraction were prepared by electopolishing sections of the material which were cut from the bulk material by spark discharge. The electropolishing solution was 62.5% methanol, 31% butanol and 6.5% of 70% perchloric acid at 13.9 volts and -40 to $-50^{O}C$. For transmission electron microscopy and selected area electron diffraction a Phillips 200 transmission electron microscope was used with an excitation voltage of 100 Kv. For thick specimens, a JOEL transmission electron microscope was used with an excitation voltage of 200 Kv. Phase structure and lattice parameters of α-Ti, β-Ti, α′-Ti martensite, were determined by selected area electron diffraction.

On some thermally treated specimens electron probe microanalysis was performed to determine the elemental chemistry of the phases. This was done using an x-ray emission and energy

dispersive technique [21,22]. Mass fractions of elements were calculated utilizing FRAME developed at the National Bureau of Standards [23,24]. Specimens for electron probe microanalysis were mounted, mechanically polished to a 0.05 μM (alumina powder) surface finish and etched very lightly with Kroll's etchant. The electron probe microanalysis was performed with an Applied Research Laboratory EMX electron probe microanalyzer. An optical microscope, attached with the electron probe microanalyzer, was used to locate the area for analysis. The electron beam diameter used was 0.5 micron and the analytical volume was 1.5 to 2 cubic microns.

TEST RESULTS

Gilmore and Imam showed that of the annealed microstructures, α-β annealed, recrystallization annealed and β annealed, the α-β annealed microstructure demonstrated the longest fatigue life [2]. On the basis of this research, the α-β annealed microstructure was utilized as a standard in this investigation for a comparative study.

The mechanical test results are presented first and followed by the results from microstructural analysis which includes optical and electron microscopy, electron probe microanalysis and x-ray analysis.

Results of fatigue life studies to final fracture are presented in Table I. An observation from the table was all of the quenched microstructures showed a significant increase in fatigue life relative to the annealed alloy, but the most striking observation was that at a heat treatment temperature of 900°C (1650°F) there was an increase by a factor of four in fatigue life relative to the other thermal treatment temperatures, and a factor of ten increase relative to the α-β annealed specimens. Strain vs cycles to failure curves determined for α-β annealed specimens and the specimens heat treated at 900°C (1650°F) are shown in Figure 4. These curves show that particularly at high strain amplitude the material heat treated at 900°C demonstrated the longest fatigue life. Specimens given this treatment were given additional aging treatments to see if further improvement in fatigue life was possible. Specimens were heat treated at 900°C (1650°F) and water

quenched then aged at 760°C (1400°F) for one hour, and at 500°C (932°F) for eight hours. Results of fatigue life studies in torsion with a sinusoidal strain amplitude with a maximum of ±0.02 are presented in Table II. The results indicate that the fatigue life of the specimens aged at 760°C (1400°F) were essentially the same as that of the α-β annealed specimens; the fatigue life of the specimens aged at 500°C (932°F) were reduced by a factor of seven relative to that of the as quenched condition, but the life was still greater than that of the α-β annealed material. Thus, the aging of Ti-6Al-4V alloy quenched from 900°C (1650°F) did not improve the fatigue life; rather, the aging reduced the fatigue life implying that the as quenched microstructure was more desirable from a fatigue life view point.

Because the specimens heat treated at 900°C and water quenched demonstrated the longest fatigue life when tested in torsion; specimens of this treatment were tested in constant stress amplitude tension-compression fatigue to see if the results were similar for this type of loading. The results of these tests are presented in Table III. These results show that the fatigue life of the specimens heat treated at 900°C followed by a water quench was approximately forty times longer than the fatigue life of the α-β annealed specimens. Thus, the two heat treatments showed an even larger difference in fatigue life when tested in the tension-compression mode (stress control) than with the torsion mode (strain control) tests. It is noted that the torsion fatigue tests were done in completely reversed strain cycles (R= -1)

whereas tension-compression fatigue tests were conducted in stress control with R = -0.3, hence, direct correlation of these results was not attempted.

The results of the tensile tests are presented in Table IV. The tensile test results show that the material heat treated below the β transus temperature (~900°C) followed by a water quench exhibited good ductility. The material solution treated above the β transus temperature followed by a water quench showed poor ductility. Among all the quench treatments the material heat treated at 900°C exhibited the highest Young's modulus and the best ductility. The Young's modulus was determined by measuring the slope of the stress-strain curve and we estimate that these elastic moduli were determined to within ±3%. The tensile strength and yield strength of heat treated alloys were comparable except for the alloy heat treated at 843°C which had a significantly lower yield strength. This low value of yield strength in the alloy heat treated at 843°C is in agreement with the results of Sherman and Kessler [18]. The main conclusion of the tensile test was that the alloy heat treated at 900°C and water quenched had relatively high strength and ductility properties.

The results of the microhardness measurements are presented in Table V. They show that the material heat treated at 843°C followed by a water quench had a hardness of 380 HK_{100} which was lower than the α-β annealed material which had a hardness of 434 HK_{100}. The microhardness increases regularly with the increase

in the thermal treatment temperature up to the beta transus temperature where the rise in microhardness tapers off. These microhardness results were in agreement with those of Fopiano et al.[19].

The tests of tensile properties and microhardness provide no significant indication of why the material heat treated at 900°C would result in order of magnitude increases in fatigue life. The microstructural analysis of Fopiano et al.[19] indicated a continuous decrease in the amount of α' relative to α as heat treatment temperature was decreased with no discontinuities that could explain our observed increase in fatigue life. The results of Williams and Blackburn [25] indicate much different phases present than the results of Fopiano et al.[19]. Williams and Blackburn found that for heat treatment temperatures just above 900°C martensite, β , and primary α all existed; however, below 900°C only martensite and primary α existed. Because of the disagreement in the literature concerning the phases present as a function of heat treatment temperature, it was necessary to study the microstructures of these specimens in detail. Particular emphasis was placed on the alloy heat treated at 900°C. The transmission electron micrograph of the α-β annealed material in Figure 5 shows that the microstructure has a mixture of grain boundry beta phase with primary alpha as the main constituent. Optical and transmission electron micrographs of an alloy specimen heat treated at 843°C and water quenched are shown in Figures 6 and 7. The microstructure was a mixture of retained beta (29 volume percent)

and primary alpha. A few regions of martensite were also observed. Selected area electron diffraction was used in the microstructural analysis.

The alloy heat treated at 900°C was investigated thoroughly because it resulted in the longest fatigue lives of the various treatments applied to the alloy Ti-6Aℓ-4V. Optical and transmission electron micrograpns of Alloy 2 heat treated at 900°C and water quenched are shown in Figures 8 and 9. From the optical micrograph the dark α-Ti phase was determined to be approximately 50 volume percent of the total. The transmission electron micrograph in Figure 9 shows that one phase was a mixture of α′-Ti and retained β-Ti the other phase was the α-Ti grains. The phases were identified by the technique of selected area diffration. The morphology of the martensite was observed in the dark field image of Figure 10 taken of a martensite reflection. From the standard TEM and the dark field image it appeared that approximately 50 volume percent of the matrix had transformed to martensite and approximately 50 volume percent remained as retained β. Note that on the polished and etched surface in Figure 8 of the as quenched alloy there was no evidence of surface relief.

Some of the specimens that were heat treated at 900°C and water quenched were subsequently aged. The optical and transmission micrographs of these specimens aged for 1 hour at 500°C, 8 hours at 500°C and 1 hour at 760°C are presented in Figures 11 through 16. In the alloy aged for 1 hour at 500°C (see the TEM of Figure 12) the nuclei that were present after quenching (Figure 9) appeared to grow in the retained β matrix. Also after aging for one hour, surface

relief was observed on the polished and etched surface in Figure 11. Because of the lath morphology of the new phase and the appearance of surface relief we conclude that the new phase was martensite. This conclusion was supported by a microhardness measurements in Table V from the aged material. After one hour at 500°C the hardness was much higher than the hardness of the as quenched material and it was much higher than the hardness of α' quenched from 1065°C. If the nuclei were α instead of α' such an increase in hardness would not be expected.

In a related experiment, transmission electron micrographs were obtained from Alloy No. 2 in the as quenched from 900°C condition following failure in tension-compression fatigue (discussed above). Figure 17 shows that after cycling there was a lath like phase that had a HCP structure based upon selected area diffraction. The lath like phase appeared to be martensite formed by a strain induced transformation from retained β. The strain induced martensite in Figure 17 and the phase formed after a 1 hour age at 500°C in Figure 12 were of similar morphology.

Aging the 900°C as quenched Alloy No. 2 for 8 hours resulted in the optical microstructure shown in Figure 13. The surface relief was also apparent in this figure. Selected area diffraction of the lath microstructure observed in Figure 14 indicated a hexagonal close packed structure, this structure appears to be the growth product of the phase observed after one hour at 500°C. No body centered cubic β phase could be detected.

It was concluded that the lath phase observed after 8 hours of aging at 500°C was tempered martensite. This conclusion was supported by microhardness measurements in Table V, the 8 hour aged specimen hardness was less than that observed after 1 hour indicating a tempering type of process. The TEM in Figure 16 of the alloy tempered for 1 hour at 760°C shows that the microstructure consisted of large grains of primary α and a region that appeared to be of Widmanstätten type microstructure. Initially this latter region was retained β plus α' and during the aging it transformed to the Widmanstätten α plus grain boundary β

The optical and T.E. micrographs of the alloy heat treated at 927°C and water quenched are shown in Figure 18 and 19. The optical micrograph in Figure 18 showed that this alloy was quite similar to the alloy heat treated at 900°C except that the primary α phase has decreased to about 40 volume percent and surface relief can be observed in the as quenched matrix phase. The TEM in Figure 19 showed that a significant change occured in the matrix; about 77% of the β phase had transformed to α' martensite during the water quench.

An optical micrograph of the alloy heat treated at 954°C and water quenched is shown in Figure 20. This microstructure appeared to be 100% α' martensite. This temperature was apparently very close to the β transus because no primary α appeared in the micrograph. This optical microstructure was quite similar to that obtained in Figure 21 by heat treating at 1065°C and water quenching; and 1065°C was at least 80°C above the transus. The TEM of the martensite formed by water quenching from 1065°C in Figure

22 showed that this martensite was quite coarse in comparison to that observed in alloys quenched from temperatures below the transus.

Electron probe chemical microanalysis was determined in the phases present in alloys water quenched from 843°C, 900°C, 927°C and 1065°C. This information was desired for correlation with phase stability. The data presented in Table VI and plotted in Figure 23 showed that as the heat treatment temperature was increased the β phase became leaner in β stabilizer (V). When the β phase that was lean in β stabilizer was quenched it was more likely to be unstable and transform to martensite. This explains why after water quenching from 843°C, 900°C, 927°C, 954°C and 1065°C the percentage of β that transformed increased from 10 to 100 percent. The lattice parameters of the phases present after quenching from 1065°C and 900°C are presented in Table VII.

DISCUSSION

The detailed microstructural analysis utilizing TEM and electron probe microchemical analysis permits an understanding of the mechanical properties observed. The increased fatigue life and high ductility of the alloy heat treated at 900°C and water quenched was a result of a strain induced transformation of β to α′. After the water quench the most unstable β phase material had transformed to α′martensite. This material was probably low in vanadium and high in localized strain. The retained β phase material although more stable than the material that had transformed was in a metastable condition and could transform to α′ if activated. The retained β obviously had a significant amount of stability as demonstrated by high yield strength and the high elastic modulus in the tensile tests. The metastable retained β was activated for transformation by both mechanical and thermal energy. The metastable retained β transforms during fatigue cycling to martensite. This mechanism of deformation apparently occurs rather than dislocation motion that leads to crack initiation. Once the β phase was fully transformed to martensite then the normal fatigue mechanisms resumed; this conclusion was supported by the relatively lower fatigue lives of alloys containing the α′ phase, and the higher fatigue life of the alloy with retained β that transformed during cycling.

The experimental observations indicated that the β retained after quenching from 900°C could also be thermally activated to transform into α′ martensite, thus this martensitic transformation

must be isothermal in character. Williams' recent review article emphasized that the martensitic transtormation of the β phase Ti and its alloys was athermal, and that no valid isothermal transformations had been observed [26]. Therefore; it is necessary to prove conclusively that the transformation observed was an isothermal martensitic transformation. The aging experiments of the β retained after the water quench conclusively show that the transformation was isothermal. The more difficult part to prove is that it was a martensitic transformation. There is a significant amount of evidence that the result of the transformation was martensite:

a. The fine lath morphology of the transformation product after aging for 1 hour at 500°C.
b. The high microhardness after aging for 1 hour at 500°C.
c. The absence of surface relief in the optical micrograph of the specimen as quenched from 900°C and the appearance of surface relief with aging at 500°C for 1 hour and 8 hours.
d. The morphological similarity of the strain induced martensite and the isothermal transformation product.
e. The absence of any detectable β phase resulting from nucleation and growth after aging the 900°C as quenched material for 8 hours at 500°C.

Williams has observed that the retained β phase transforms directly to Widmanstätten α phase that obeys the Burgers relationship [26]. The results of our work show that the β phase that

was retained after a water quench from 900°C transformed by an isothermal martensitic transformation to α'. Continued aging of the martensite resulted in a tempered martensite. It is expected that the tempered martensite would eventually transform to equilibrium α plus β of the Widmanstätten type structure.

It was interesting to go back to the original paper by Wiskel **et** al. where the kinetics of the β to α phase transformation was first reported [27]. Wiskel et al. cooled high purity titanium from 1000°C at a rate of 2°C per minute. They reported that "these structures presumably indicate a shear transformation β → α athermally nucleated, but capable of isothermal progression." This appears to be what we were observing in this 900°C alloy. In the as quenched condition nuclei can be observed that formed during the quench. Then the TEM's after 1 hour and 8 hour aging at 500°C depict the isothermal growth of the nuclei that formed on quenching. This type of model is that of an isothermal martensite. However, in the literature Wiskel's work is quoted as evidence that the β to α transformation is athermal [28]. From the work reported by Wiskel et al. it could be concluded that even in pure titanium the β to α transformation was isothermal.

The results of the microstructural and microchemical analysis are internally consistent and provide a rationale for understanding the transformations observed in this alloy. When this alloy was solution treated above the β transus the entire alloy eventually became fully β and the α and β stabilizers were uniformly distributed throughout the β phase. Because this was a lean β

alloy the β phase was insufficiently stable for retention during the water quench and a β to α´ martensite transformation resulted. At heat treating temperatures below the β transus both α and β phases exist in equilibrium. The α phase that forms rejects the β stabilizing element (V). The lower the temperature below the β transus, the greater the amount of α and thus the greater the amount of rejected β stabilizer into a decreasing amount of β. At 900°C there was sufficient β stabilizer present that a significant amount of the β phase was retained during quenching. Further reduction in heat treating temperature to 843°C resulted in a further decrease in the amount of retained β before the water quench, and the β phase was sufficiently β stabilized by the vanadium rejected from the α phase that during the water quench much of the β was retained. This rationale is supported by the microstructural and microchemical results in Table VI and Fig. 23.

It is necessary to explain why our microstructural results were significantly different than those of some previous authors. Averbach, Comerford and Bever did not observe any retained β following water quenching from heat treatment temperatures over the same range as in our experiments [29]. One difference in their procedure was that all of their specimens were given a prior solution treatment at 1005°C (1840°F) and the specimens were water quenched. During the quench all of the β should have transformed to martensite. The specimens were then heat treated at temperatures from 1005°C to 800°C for one hour and water quenched a second time. In their work it is quite possible that the

martensite structure formed after the first quench did not revert to the β phase during subsequent aging because it is well known that the $\alpha \rightarrow \beta$ transportation is quite slow at temperatures close to the β transus. The work of Fopiano, Bever, and Averback [19] came to a similar conclusion as that of Averbach, Comerford, and Bever; that no β phase was retained after water quenching from heat treating temperatures below the β transus. The experiments of Fopiano [19] appear to be identical to our experiments because no prior solution treatment was reported and yet the results were significantly different. Their experiments utilized the techniques of x-ray diffraction, and electron microscopy. However, Fopiano et al. do not report any selected area electron diffraction and in our work this was the primary technique utilized to identify the retained β phase. X-ray diffraction techniques could not detect the retained β phase, and the reason for this is not clear.

Another result from this work that is significantly different from those reported by Fopiano is the microchemistry of the phases after water quenching. However, the results reported here were experimental, and the results presented by Fopiano were based upon estimated phase diagram tie lines [19].

There are some differences and agreement of our results and the work of Williams and Blackburn [25], but their work was qualitative so the extent of agreement or disagreement is hard to evaluate. Williams and Blackburn report that β phase was retained after water quenching from all temperatures from 1100°C to 800°C except for a small temperature range from approximately 860°C to

900°C. We observed that after quenching from above the β transus all of the β transformed to α′during the quench. A reduction of heat treating temperature to below the β transus resulted in less β phase, but the increase in β stabilizer (V) rejected from the α phase caused the β phase to be more stable. Williams and Blackburn also differentiated between α′ (hexagonal martensite) and α′′ (orthorhombic martensite). We were unable to distinguish the difference between α′ and α′′ in the Ti-6Aℓ-4V alloy. Williams has noted that it was possible to distinguish between α′ and α′′ only with vanadium concentrations of about 14 weight percent or higher where the lattice distortion was sufficient to detect [30]. Also Williams has noted that the strain induced transformation of retained β to martensite always produces the orthorhombic α′′[26]. Our work showed that after water quenching from 900°C the morphology of the strain induced product was significantly different than the α′which is the product of quenching from above the β transus, where the α′phase contained large packets of parallel martensite laths. The strain induced martensite had smaller individual laths which intersected with laths oriented along different axes. This latter microstructure could be that of the α′′. The microstructure resulting from isothermal transformation of the β retained after water quenching from 900°C was similar to that induced by a strain, thus it is possible that the isothermal transformation product was also α′′.

CONCLUSIONS

1. Specimens heat treated at 900°C and water quenched exhibited increased fatigue lives, high ductility, yield strength and elastic modulus when compared with other heat treating temperatures or anneal procedures.

2. The increased fatigue life and high ductility resulting from quenching from 900°C was due to a strain induced martensitic transformation of retained β to α′ martensite.

3. Isothermal aging of retained β resulted in a thermally activated martensitic transformation of retained β to α′ martensite, this indicated that the retained β transformed by an isothermal martensitic transformation to α′ martensite.

4. The microstructures present after quenching from heat treatment temperatures were explained by considering the amount of β stabilizer present in the β phase. The lower the heat treatment temperature below the β transus the more equilibrium α present relative to β . The α phase rejected β stabilizer α the lower the heat treatment temperature the more β stabilizer rejected from α into a lesser amount of β phase. Lower heat treating temperatures thus produced smaller amounts of more stable β phase. Higher heat treating temperatures produced greater amounts of less stable β phase that tended to transform to martensite during quenching.

ACKNOWLEDGEMENT

The authors acknowledge the financial support provided by the Naval Air Systems Command. The authors also thank the staff at The National Bureau of Standards for permitting the use of their microscopy and microanalysis facility, and specially to Dr. Anna Fraker for her assistance. Discussions with Dr. George Yoder of The Naval Research Lab were of considerable help during the progress of this work.

REFERENCES

1. R. C. Steele and A. J. McEvily, 3rd International Conference on Titanium, Moscow State University, USSR, May 1976, 131 (Abstracts).
2. C. M. Gilmore and M. A. Imam, 3rd International Conference on Titanium, Moscow State University, USSR, May 1976, 139 (Abstracts).
3. R. A. Sprague, D. L. Ruckle, and M. P. Smith, Titanium Science and Technology, ed. R. I. Jaffee and H. M. Burte, Plenum Press, 1973, Vol. 3, 3069.
4. M. A. Greenfield, C. M. Pierce, and J. A. Hall, Titanium Science and Technology, ed. R. I. Jaffee and H. M. Burte, Plenum Press, 1973, Vol. 3, 1731.
5. M. Raefsky, Boeing-Vertol Internal Report D8-1041,(May 1970).
6. L. J. Bartlo, ASTM STP459 (1969) 144.
7. J. E. Coyne, The Science, Technology and Application of Titanium, ed. R. I. Jaffee and N. E. Promisel, Pergamon Press, 1970, p. 97.
8. E. Beck, MCR-69-140 to AFML, WPAFB , Ohio, (May 1970)
9. M. Tiktinsky, The Science, Technology and Application of Titanium, ed. R. I. Jaffee and N. E. Promisel, Pergamon Press, 1970, 1013.
10. J. J. Lucas, Titanium Science and Technology, ed. R. I. Jaffee and H. M. Burte, Plenum Press, 1973, Vol. 3, 2081.

11. A. W. Bowen and C. A. Stubbington, Titanium Science and Technology, ed. R. I. Jaffee and H. M. Burte, Plenum Press, 1973, Vol. 3, 2097.

12. A. M. Adair and W. H. Riemann, Titanium Science and Technology, ed. R. I. Jaffee and H. M. Burte, Plenum Press, 1973, Vol. 3, 1801.

13. A. W. Thompson, J. C. Williams, J. D. Frandsen, and J. C. Chesnutt, 3rd International Conference on Titanium, Moscow State University, USSR, May 1976, 145 (Abstracts).

14. A. W. Bowen and C. A. Stubbington, 3rd International Conference on Titanium, Moscow State University, USSR, May 1976, 404 (Abstracts).

15. R. I. Jaffee, The Physical Metallurgy of Titanium Alloys, Progress in Metal Physics, Pergamon Press, 1958, 65.

16. C. A. Stubbington and J. T. Ballett, Titanium Science and Technology, ed. R. E. Jaffee and H. M. Burte, Vol. 1, Plenum Press, 1973, Vol. 1, 601.

17. F. A. Crossly and R. E. Lewis, Report LMSC-D356114, (1973).

18. R. G. Sherman and H. D. Kessler, Trans. ASM, 1956, Vol. 48, 47.

19. P. J. Fopiano, M. B. Bever, and B. L. Averbach, Trans. ASM, 1969, Vol. 62, 324.

20. ASTM Specification E8, 1971, p. 205.

21. K. F. J. Heinrich, NBS Technical Note 719, (Appendix II, NBS Technical Note 521), May 1972, 35.

22. R. Castaing, Doctoral Thesis, University of Paris, (1951).

23. H. Yakowitz, R. L. Myklebust, and K. F. J. Heinrich, NBS Technical Note 796, (October 1973).

24. J. Philibert and R. Tixier, in "Quantitative Electron Probe Microanalysis", ed. K. F. J. Heinrich, NBS Special Publication 298, 1968, 13.

25. J. C. Williams and M. J. Blackburn, Trans. ASM, 1967, Vol. 60, 373.

26. J. C. Williams, Titanium Sicence and Technology, ed. R. I. Jaffee and H. M. Burte, Plenum Press, 1973, Vol. 3, 1433.

27. S. U. Wiskel, W. V. Youdelis, and J. G. Parr, Trans. Met. Soc. AIME, 1959, Vol. 215, 875.

28. M. K. McQuillan, Met. Rev., 1963, Vol. 8, 41.

29. B. L. Averbach, M. F. Comerford, and M. B. Bever, Trans. Met. Soc. AIME, 1959, Vol. 215, 682.

30. J. C. Williams, Private communication.

TABLE I

Fatigue Lives of Thermally Treated Ti-6Aℓ-4V Alloys Cycled at a Shear Strain of ± 0.02 at 0.2 Hz

Thermal Treatment†	Mean Life*	Minimum Life	Standard Deviation
α - β Annealed	944	429	443
HT - 843°C (1550°F) + WQ	2497	1837	717
HT - 900°C (1650°F) + WQ	9616	8917	758
HT - 927°C (1700°F) + WQ	2223	2142	605
ST - 1065°C (1950°F) + WQ	2396	1633	487

†HT: Heat treatment for 10 minutes
ST: Solution treatment for 10 minutes
WQ: Water quench

*Results based upon four specimens for each thermal treatment

TABLE II

Fatigue Lives of Heat Treated (900°C) and aged (500°C and 760°C) Ti-6Aℓ-4V Alloys Cycled At a Shear Strain of ± 0.02, A Frequency of 0.2 Hz

Thermal Treatment†	Mean Life*	Minimum Life	Standard Deviation
HT - 900°C + WQ	9616	8917	758
HT - 900°C + WQ + 500°C Temper 8 Hours	1423	935	486
HT - 900°C + WQ + 760°C Temper 1 Hour	852	745	122

†HT: Heat treatment for 10 minutes
WQ: Water quench

*Results based upon four specimens for each thermal treatment.

TABLE III

Fatigue Lives for Tension-Compression Tests
With σ_{max} = 827 MPa (120 ksi), R = -0.3

Thermal Treatment†	Test #1	Test #2
α - β Annealed	20,836	10,777
HT - 900°C + WQ	1,005,456	499,556

†HT: Heat treatment for 10 minutes

WQ: Water quench

TABLE IV

Tensile Test Results for Ti-6Al-4V*

Thermal Treatment†	Yield Strength (±1%)MPa (ksi)	Ultimate Strength (±1%)MPa (ksi)	Young's Modulus (±1%)10^3MPa (10^6 psi)	Percentage Reduction in Area	Percentage Elongation
α - β Annealed	899 (130.46)	990 (143.60)	103 (15.00)	41.0	30.0
HT - 843°C + WQ	789 (114.50)	1059 (153.60)	88 (12.75)	40.3	24.7
HT - 900°C + WQ	998 (144.70)	1158 (167.90)	116 (16.80)	40.2	26.5
HT - 927°C + WQ	1013 (146.90)	1184 (171.70)	106 (15.40)	32.5	21.5
ST - 1065°C + WQ	1007 (146.10)	1082 (157.00)	108 (15.70)	2.1	2.5

*Results based upon two specimens for each thermal treatment.

†HT: Heat treatment for 10 minutes

ST: Solution treatment for 10 minutes

WQ: Water quench

TABLE V

Microhardness of Thermally Treated Ti-6Aℓ-4V Alloys

Thermal Treatment†	Knoop Hardness*	Standard Deviation
α - β Annealed	434	1.5
HT - 843°C + WQ	380	4.3
HT - 900°C + WQ	455	7.1
HT - 900°C + WQ Age 1 Hr. at 500°C	792	11.6
HT - 900°C + WQ Age 8 Hrs. at 500°C	547	5.1
HT - 900°C + WQ Age 1 Hr. at 760°C	447	5.5
HT - 927°C + WQ	477	6.6
HT - 955°C + WQ	504	5.3
ST - 1065°C + WQ	511	0.0

†HT: Heat treatment for 10 minutes
ST: Solution treatment for 10 minutes
WQ: Water quench

*Based upon 8 measurements

TABLE VI

Microchemistry of Thermally Treated
Ti-6Al-4V Alloys

Thermal Treatment†	Phases & Volume Percent Observed	Phase Composition Al	Phase Composition V
HT - 843°C + WQ	α (71%)	7.66 ± 0.15	2.66 ± 0.28
	β (26%) + α′ (3%)	5.99 ± 0.27	6.79 ± 0.62
HT - 900°C + WQ	α (50%)	7.49 ± 0.10	2.51 ± 0.12
	α′(25%) + β (25%)	5.80 ± 0.26	6.66 ± 0.65
HT - 927°C + WQ	α (40%)	7.02 ± 0.07	2.33 ± 0.16
	α′(46%) + β (14%)	5.62 ± 1.09	5.91 ± 0.09
ST - 1065°C + WQ	α′ (∿100%)	6.61 ± 0.90	4.74 ± 0.07

†HT: Heat treatment for 10 minutes
ST: Solution treatment for 10 minutes
WQ: Water quench

TABLE VII

LATTICE PARAMETERS OF TI-6Aℓ-4V PHASES

HEAT TREATMENT	PHASE	LATTICE PARAMETERS IN A°
1066 C. - ST + WQ	α'	a = 2.925 c = 4.634
900 C. HT + WQ	α'	a = 2.942 c = 4.738
900 C. HT + WQ	α'	a = 2.931 c = 4.696
900 C. HT + WQ	β	a = 3.299

ST: Solution treated for 10 min.

HT: Heat treated for 10 min.

WQ: Water quench

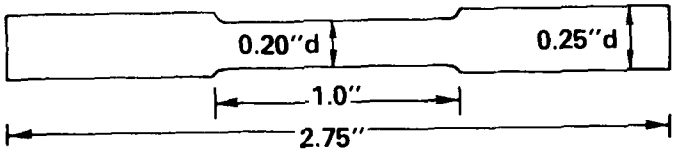

Figure 1. Torsion fatigue specimen design.

Figure 2. The machine for torsional fatigue.

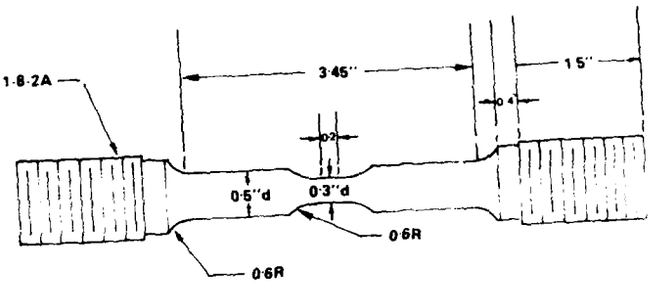

Figure 3. Tension-compression fatigue specimen design.

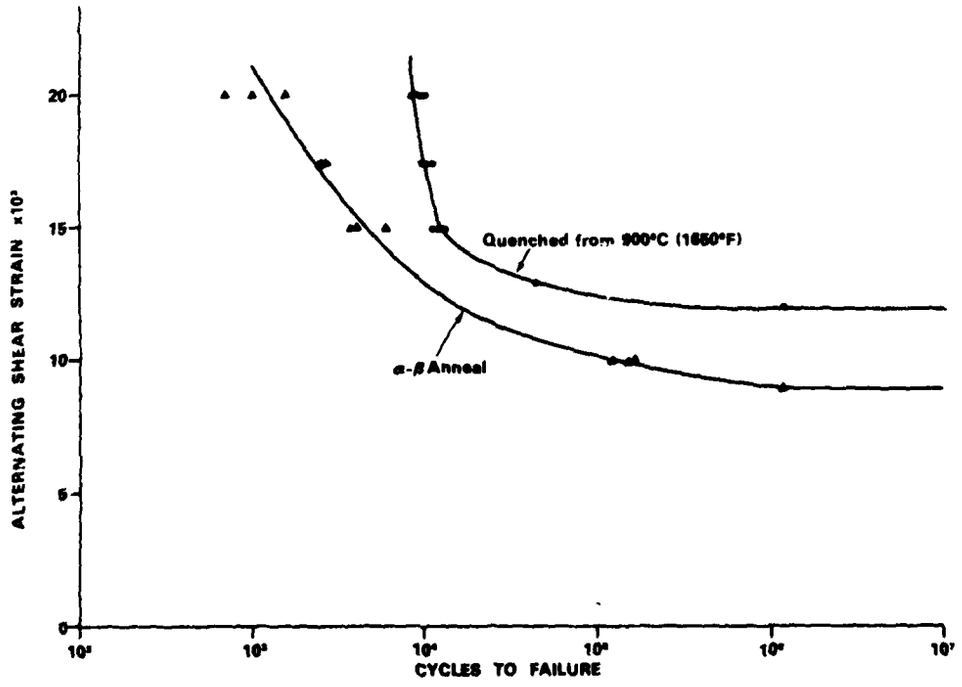

Figure 4. Cycles to failure as a function of the applied alternating shear strain for specimens α-β annealed, and heat treated at 900°C and water quenched.

Figure 5. [illegible] electron micrograph [illegible] showing [illegible] Ti grains.

Figure 6. [illegible] micrograph of Ti-6Al-4V [illegible] treated at [illegible] and water [illegible] showing α-Ti (labeled X) [illegible].

[illegible] electron micrograph [illegible] Ti-6Al-4V heat [illegible] and [illegible] showing [illegible].

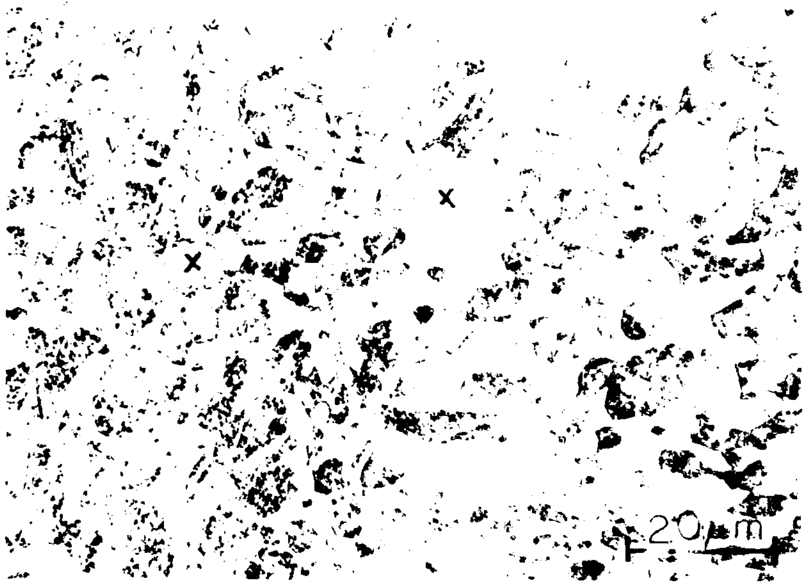

Figure 8. [illegible]ptical micrograph of [illegible] treated at [illegible]°C (1650°F) and water [illegible] showing [illegible]-Ti (labeled x) and [illegible]-Ti. [illegible] contains [illegible] Ti martensite which [illegible] here.

Figure 9. Transmission electron [illegible] heat treated at [illegible] (1[illegible] [illegible]. The diffraction pattern [illegible] the alloy that indexes as [illegible] martensite [illegible]

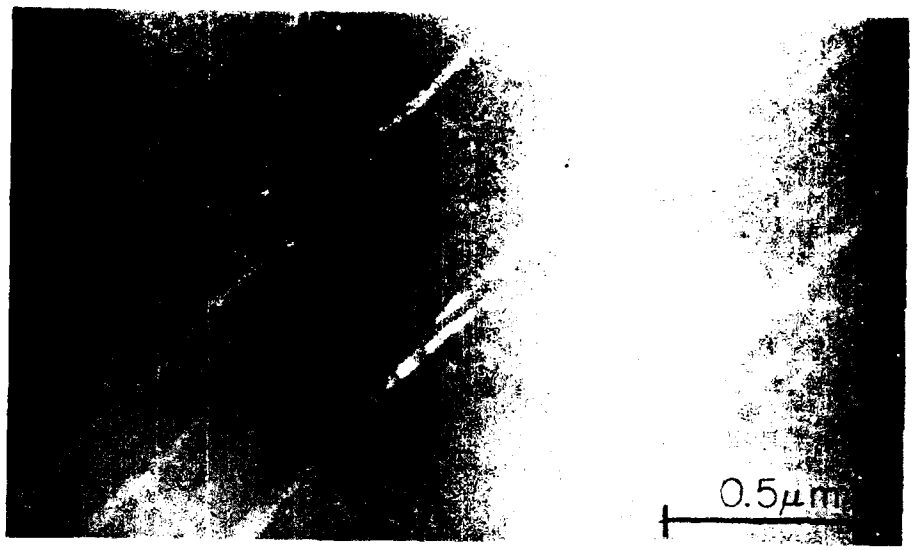

Figure 10. Transmission electron mic[illegible] of Ti-6Al-4V heat treated [illegible] and water quenched showing ta[illegible] martensite. Dark field reflect[illegible]

Figure 11. Optical micrograph of Ti[illegible] at 900°C and water quench[illegible] 590°C for one hour.

Figure 12. Transmission electron [illegible] heat treated at 900°C [illegible] by aging at 500°C for [illegible] and the phase region [illegible] grown.

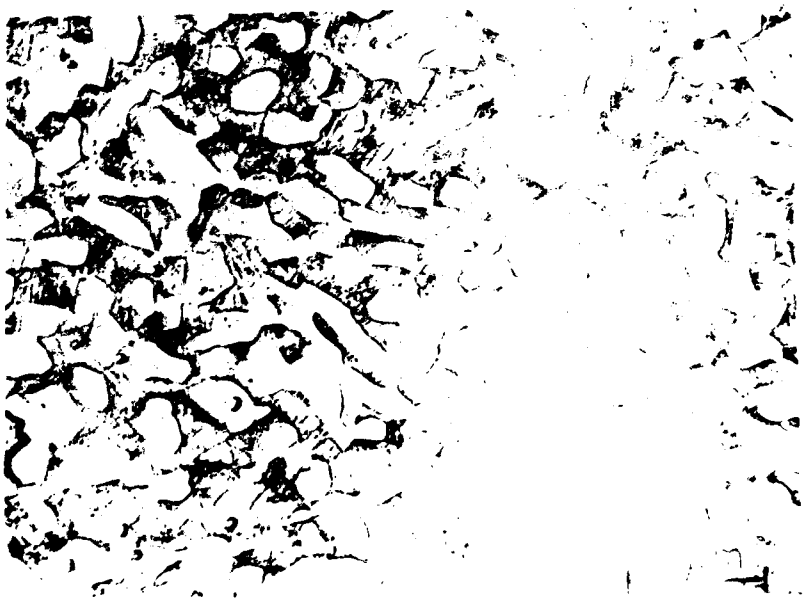

Figure 13. Optical micrograph of [illegible] 900°C (1650°F) and water [illegible] aging at 500°C for 8 hrs.

Figure 14. Transmission electron micrograph of the same specimen as in Figure 13 showing α-Ti (labeled x) and the phase region where α′-Ti martensite has grown.

Figure 15. Optical micrograph of Ti-6Al-4V heat treated at 900°C (1650°F) and water quenched followed by aging at 760°C (1400°F) for one hour.

Figure 16. Transmission electron micrograph [illegible] specimen as in Figure 15 [illegible] boundary β-Ti.

Figure 17. Transmission electron micrograph [illegible] specimen as in Figure 9 taken close to [illegible] surface after tension [illegible] showing sharp needles of [illegible] Ti grains.

Figure 18.

Figure 19.

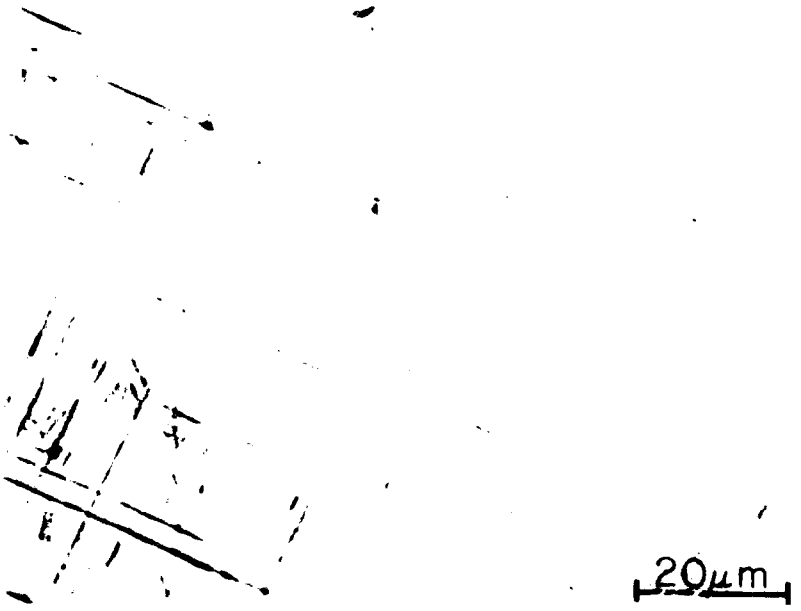

Figure 29. Optical micrograph of Ti-6Al-4V heat treated at [illegible] and water quenched showing α'-Ti martensite.

Figure 22. Transmission electron micrograph of the same specimen as in Figure 21. The electron diffraction pattern indexes to be ε' (hexagonal) martensite.

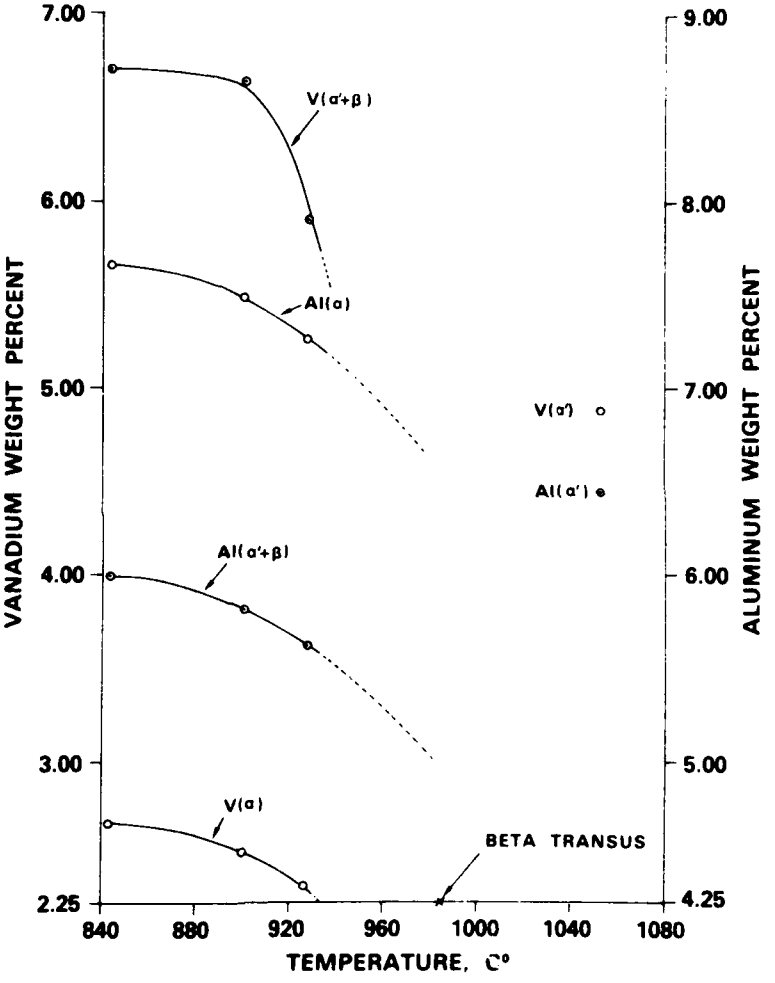

Figure 23. Microchemistry of Ti-6Aℓ-4V alloy as a function of quenching temperature. The hold time at temperature was 10 minutes.

A CRYSTALLOGRAPHIC STUDY OF FATIGUE DAMAGE IN TITANIUM

by

M. Sugano and C. M. Gilmore

School of Engineering and Applied Science
George Washington University
Washington, D.C.

ABSTRACT

Large grain specimens with average grain size of 0.0127 m made from commercial purity titanium were subjected to a torsional cyclic strain at two different amplitudes: ±0.008 and ±0.003. Fatigue damage was studied by scanning electron microscopy and crystal orientations were determined by x-ray diffraction and surface trace analysis. It was found that cyclic strain amplitude influenced the deformation mode and the nature of the macroscopic crack propagation. At high strain amplitudes the normal slip processes were observed and microcracking was observed on the (0001), and $\{1\bar{1}00\}$ slip planes. The macroscopic crack propagation was dominated by the Stage I shear mode; however, some Stage II tensile mode propagation was observed after extensive Stage I propagation. At low strain amplitude twin plane cracking was observed on the $\{10\bar{1}1\}$, $\{10\bar{1}0\}$, and $\{11\bar{2}3\}$ planes in addition to normal slip plane cracking, and the macroscopic crack propagation was dominated by the Stage II tensile mode. However, microscopic examination showed the macroscopic tensile mode cracks to be composed of microscopic shear mode cracks along slip

planes and twin planes. At both low and high strain amplitudes cracking was observed on the $\{11\bar{2}0\}$ plane which is neither a slip or twin plane in titanium. It is proposed that this cracking mode was a result of a dislocation reaction forming sessile dislocations on the $\{11\bar{2}0\}$ plane.

FIGURE CAPTIONS

Figure 1. Fatigue microcracking observed in the vicinity of a macroscopic crack. Cyclic shear strain amplitude ±0.008.

Figure 2. Cracking along a (0001) slip plane that also appears to be a subgrain boundary. Cyclic shear strain amplitude ±0.008.

Figure 3. Slip band cracking on the $(1\bar{1}00)$ and shear cracking on the $(10\bar{1}0)$. Cyclic shear strain amplitude ±0.008.

Figure 4. Severe deformation surrounding a tensile mode crack propagating on a $(11\bar{2}0)$ plane after cycling at ±0.008 cyclic shear strain amplitude.

Figure 5. Localized shear microcracking on slip and twin planes along a macroscopic tensile fatigue crack after cycling at ±0.003.

Figure 6. Localized fatigue cracking on the twin planes $(11\bar{2}3)$ and $\{11\bar{0}1\}$ after cycling at ±0.003.

Figure 7. Localized fatigue cracking on a $(\bar{1}102)$ twin plane after cycling at ±0.003.

Figure 8. The tip of a fatigue crack changing from a (0001) plane to a $(10\bar{1}0)$ plane. No slip lines were observed at the crack tip. Cyclic shear strain amplitude ±0.003.

INTRODUCTION

It is now well established that fatigue cracking in ductile metals is closely related with extrusions and intrusions which are formed in slip bands.[1-3] Fatigue deformation was generally observed to concentrate at boundaries of a grain at higher strain amplitude, while at lower strain amplitude deformation was widely dispersed over the grains.[4,5] Most of these studies were carried out on metals and alloys possessing a face centered cubic crystal structure. Published fatigue studies for metals and alloys having body-centered cubic and hexagonal close packed crystal structures are much more limited. Particularly, few studies appear in the literature on hexagonal close packed metals where mechanical twinning can become an important mode of deformation. It was shown that in pure titanium fatigue deformation and crack initiation occured at deformation twins.[6-13] Titanium is known to have a high stacking fault energy,[14,15] thus wavy slip lines might also be expected on the surface of a specimen deformed at room temperature. However, fresh twins were observed to be continuously introduced during fatigue at high strain amplitudes, and cracks originated preferentially on the twin boundaries.[8-10] Twin boundary damage was also observed at existing twins where the applied stress was insufficient to nucleate fresh twins.[9] Contrary to these observations Turner and Roberts observed slip band cracking;[16] and MacDonald and Wood observed a "slipless cracking", which originated and

propagated in a general direction of maximum shear.[17] It was further shown by Dickson et. al. that the major cyclic deformation mode was by slip, and that twins occupied less than 10 pct of the surface area even at a total strain amplitude of ±1.0 pct.[18]

The present study was conducted to obtain crystallographic information on the deformation mode appearing in commercial purity titanium during torsional fatigue because there does not appear to be general agreement in the literature concerning fatigue damage in titanium. We studied the fatigue damage at low (±0.003) and high (±0.008) strain amplitudes that would produce fatigue failure in approximately 1.5×10^6 and 1×10^4 cycles respectively.

EXPERIMENTAL PROCEDURE

The material for this study was commercial purity titanium tube (A40) of 0.0064 m o.d. and 0.0048 m i.d. supplied by Superior Tube Co. The chemical composition in weight percent was: carbon (0.016), iron (0.112), nitrogen (0.0084), oxygen (0.228), hydrogen (0.0075), titanium (remainder). After cutting to the length of 0.082 m, the as-received specimens were mechanically polished on emery papers through 4/0. The specimens were then heat treated in vacuum to obtain large grained specimens in a short time.[19]

After annealing for two hours at 840°C, the specimens were held for seven minutes in a temperature gradient furnace and then air cooled to room temperature. The furnace was controlled to be 945°C at the hottest point, having a temperature gradient of approximately 2°C/mm. Full annealing followed for two hours at 945°C without any temperature gradient. The average grain size was 0.0127 m in diameter and the grains ran completely across the specimen thickness.

The gauge length of the specimens was electropolished in an electrolyte consisting of 10 parts methanol, 7 parts n-buthanol and one part perchloric acid. Electropolishing was carried out for ten minutes at a maximum temperature of -20°C and at a potential of 30 Volts (D.C.).

The fatigue tests were performed on machines that produced a reversed (R=-1) sinusoidal strain at .2 Hz frequency for high

amplitude fatigue and 28 Hz frequency for low amplitude fatigue. The yield strain of this material was approximately 0.006 in torsion and the shear fatigue limit was approximately ±0.002 shear strain. All tests were conducted at room temperature.

The crystal orientation of the grains was determined by the x-ray back reflection Laue method designed so that x-ray photographs and optical micrographs can be taken from the same area. Metallographic observation was also carried out by scanning electron microscopy. Trace analysis techniques[20] were used to investigate fatigue deformation from a crystallographic point of view. Specimens were mounted on the specimen holder of the SEM with the horizontal direction parallel to their longitudinal axis, so that comparisons can be made easily between the crack propagation directions and the applied stress directions. The directions of maximum shear stress were horizontal and vertical and the directions of maximum tension and compression were at 45° to the horizontal. All photomicrographs of specimens in this paper were mounted such that the specimen axis is horizontal in the photomicrograph.

RESULTS

1. High Amplitude Fatigue -- Macroscopic crack propagation produced by high amplitude torsion fatigue testing occured in two ways; one was along the planes of maximum shear stress (shear mode crack), which were perpendicular to and parallel with the specimen axis, and the other was along the direction of the maximum tensile stress (tensile mode crack). The photomicrographs taken from shear and tensile cracks show different features. It was found that fatigue deformation was crystallographic around shear cracks, and it was observed that tensile cracking was accompanied by a severe deformation that was difficult to relate to any particular crystallographic direction. Photomicrographs taken from vicinity of macroscopic shear cracks are shown in Figs. 1 to 3. Figs. 1 to 3 were taken about 0.1 mm from the main shear crack. Fig. 1 is a typical example of cracks propagating in slip bands. It was observed that shear mode fatigue cracks ran zigzag on the $\{1\bar{1}00\}$ and (0001) slip planes which are the primary and secondary slip planes respectively in titanium.[21] The crack propagation directions were very close to that of the maximum shear stress: vertical and horizontal directions in the photographs. It can be seen in Fig. 2 that a crack propagated along the subgrain boundary formed on a (0001) plane. It is very interesting to see that fatigue deformation can be observed in the subgrain sited on right side of the crack, while on left side of the crack much less deformation was observed. This showed that plastic deformation at a

fatigue crack was strongly affected by grain orientation. Fig. 3 is a micrograph taken from a region close to the main crack. It can be observed that parallel slip bands were formed on the $(1\bar{1}00)$ planes with uniform spacing. Note that the slip bands have been bent around an axis which is perpendicular to the plane of the paper. Cracks were observed to form across the slip bands by localized shear on the $\{10\bar{1}0\}$ plane.

Figure 4 shows the microstructure around a $\{11\bar{2}0\}$ tensile mode crack. The $\{11\bar{2}0\}$ plane is not a normal slip or twin plane in titanium. Comparison of Fig. 4 with Fig. 2 shows that deformation near the tensile mode crack was more severe than that near the shear mode crack. Again in Fig. 4 it was observed that fatigue deformation on one side of the crack was more severe than that on the other side.

2. Low Amplitude Fatigue -- At the low strain amplitude the fatigue cracks probably initiated in the shear direction (Stage I), but all of the observed propagation of the macroscopic crack occured at 45° to the specimen axis in the direction perpendicular to the maximum tensile stress (Stage II). A macroscopic Stage II crack, however, did not always propagate normal to the tensile stress when viewed microscopically. For example, Fig. 5 is a micrograph taken of a section of a Stage II crack; however, microscopically the Stage II cracking occured by the linking of cracks on planes that were close to the maximum shear directions.

In Fig. 5 a small microcrack can be observed on the $(11\bar{2}3)$ plane which is a twin plane. Fig. 5 also demonstrated the cracking on the (0001) and $\{10\bar{1}0\}$ slip planes. Again cracking on the $\{11\bar{2}0\}$ plane was observed, this plane is neither a slip or twin plane. Another example of cracking along a $(11\bar{2}3)$ twin plane is shown in Fig. 6. In Fig. 6 it appears as though shear deformation on the $(11\bar{0}1)$ plane, which can be either a slip or twin plane, has displaced two segments of the crack on the $(11\bar{2}3)$ twin plane. A similar type of displacement was observed along the $(10\bar{1}0)$ slip plane on Fig. 3. These shear strains apparently occured during crack propagation. Cracking was observed on two twin planes: the $\{11\bar{2}3\}$ in Fig. 5, and the $(\bar{1}102)$ in Fig. 7.

The extensive formation of intrusions, extrusions and persistent slip bands that lead to fatigue cracking in fcc metals was not observed at low strain amplitudes in titanium. Usually at low strain amplitude there was no observed plastic deformation along the crack; the plastic deformation, if any, must have occured in the plane of crack propagation. Fig. 8 shows the tip of a propagating crack that appears to have changed from a (0001) slip plane to a $(10\bar{1}0)$ slip plane. No plastic deformation was observed around the crack tip except that in the direction of propagation.

DISCUSSION

The fatigue cracking observed in this study was in all cases crystallographic. When a primary slip system was favorably oriented along the direction of the maximum shearing stress slip band cracks formed. Cracks were observed on the following planes which are known to be slip planes: $\{10\bar{1}0\}$, (0001) and $\{10\bar{1}1\}$. In some cases dispersed slip bands, as in Fig. 3, were observed that resembled the fatigue slip bands that have been observed in fcc metals. However, in numerous cases localized cracking was observed to occur on slip planes and examples were shown of localized cracking on all of the major slip planes. The term "slipless cracks" has been applied to fatigue cracks observed in titanium alloys that occur without the formation of a persistent slip band of observable width. The "slipless cracks" observed by MacDonald and Wood in titanium appeared not to form by the mechanisms of intrusion and extrusion formation as had been observed in slip bands of fcc metals.[17] In this work the localized cracks did form on slip planes such as $(10\bar{1}0)$, (0001), and $(10\bar{1}1)$ as can be observed in Figs. 3, 5 and 7. Thus it is likely that the mechanism of the localized cracking in these specimens does include slip. We can speculate as to how localized slip band cracking might have occured.

It has been shown by Stevenson and Breedis that cyclic softening occurs during room temperature cyclic deformation of commercial purity titanium.[13] Cyclic softening was observed to occur at small cyclic plastic strain amplitudes (below ± 0.006 normal strain). If a slip band was to soften as a

result of cyclic deformation rather than harden, then we would expect subsequent cyclic deformation to concentrate in the softened slip band rather than spread to other slip bands. A slip band could become soft if dislocations were created by a source in the slip plane and cross slip and intersecting slip systems were not activated to harden the slip band. This argument is supported by the observation of Stevenson and Breedis that cyclic softening occured primarily at low strain amplitude where less cross slip and fewer active slip systems would be expected in titanium.

In addition to slip band cracking we observed cracking along twin planes of the type $\{10\bar{1}2\}$ and $\{11\bar{2}N\}$ N= 1 to 3. In this work N = 3 was the twin plane most frequently observed. Twin plane cracking can also produce a localized crack with no apparent slip; thus many of the twin plane cracks that we observed would resemble "slipless cracks". Twin plane cracking was only observed at low strain amplitudes.

In pure titanium deformation twins have been reported earlier on $\{10\bar{1}2\}$ and $\{11\bar{2}N\}$ (n=1 to 4) planes, but never on other planes.[22] However, $\{10\bar{1}1\}$ transformation twins have also been observed in the martensite of commercial purity titanium.[23] According to the Burgers' relationship of the bcc to hcp transformation[24], it is plausible that $\{10\bar{1}1\}$ type twin formation is associated with the β to α transformation in pure titanium, because the $\{10\bar{1}1\}$ plane in hcp (α phase) corresponds to the $\{110\}$ plane in the matrix (β phase). It appears, therefore, that a $\{10\bar{1}1\}$ type twin is formed during transformation but not

by deformation. These pre-existing twins might sometimes play an important role in cracking on a $\{10\bar{1}1\}$ plane.

It has been shown that twinning in pure titanium showed a general tendency to occur with increased grain size and purity and with a decrease in temperature.[25] Concerning the effect of grain size on twinning and twin fragmentation, a search of available literature disclosed that the critical grain size for twin formation appeared to be between 0.05 mm and 0.1 mm [8,3,11,13,16,18] and [26]. This indicates that the very coarse-grained specimens used in this work were above the critical size for twinning to occur during fatigue deformation.

Twin formation has also been known to be favored by a higher strain rate. Twin plane cracking was more prevalent at low strain amplitude, where a higher frequency was employed. It appears, however, that frequency was not the major influence because twinning was not observed in the case of fatigue tests performed at a higher frequency than in the present work.[1]

Cracking was observed on the $\{11\bar{2}0\}$ plane which is neither a normal slip plane nor a twin plane. It is possible that a sessile $\frac{a}{3}\{\bar{1}100\}$ dislocation lying on the $\{11\bar{2}0\}$ plane caused the brittle cracking observed in Figs. 4 and 5. This dislocation can be produced by the following reaction.[14]

$$\frac{a}{3}[2\bar{1}\bar{1}0] + \frac{a}{3}[11\bar{2}0] \rightarrow \frac{a}{3}[\bar{1}100] + \frac{a}{9}[\bar{2}110] + \frac{2a}{9}[11\bar{2}0] .$$

The cracking observed in these large grained specimens appeared to be in all cases crystallographic. However, Wood

and his associates[17] observed cracking in fine grained commercial purity titanium that appeared to be noncrystallographic. It is quite likely that the results of this work on large grained specimens is not applicable to the fine grained specimens utilized by Wood and his associates.

CONCLUSIONS

1. The magnitude of the cyclic strain amplitude influenced both the macroscopic and the microscopic character of the fatigue cracking.
2. At high strain amplitude an extensive amount of Stage I crack propagation was followed by Stage II crack propagation.
3. At low strain amplitude no macroscopic Stage I crack propagation was observed, all macroscopic crack propagation was in the Stage II tensile mode.
4. In general, microscopic cracks occured in the two principle shear directions even when the macroscopic crack was of the Stage II tensile mode. An exception to this was the observation of cracks on the $\{11\bar{2}0\}$ planes which are neither slip or twin planes in titanium, cracks on these planes tended to be oriented normal to the maximum tensile strain. This indicates cracking on these planes was of a cleavage type. Cracking on $\{11\bar{2}0\}$ planes was observed both at low and high strain amplitudes.
5. At high strain amplitudes microscopic cracking occured on the slip planes (0001) and $\{1\bar{1}00\}$.
6. At low strain amplitudes microscopic cracking occured on the (0001) and $\{1\bar{1}00\}$ slip planes; in addition twin plane cracking was observed on $\{11\bar{2}3\}$, $\{\bar{1}102\}$ and the $\{1\bar{1}01\}$ which is both a possible slip and twin plane.

7. All microscopic cracking that was observed was crystallographic; however, at high strain amplitude slip around crystallographic tensile mode cracks could not be related to any particular crystallographic plane.
8. Localized slip band cracking was observed at low strain amplitude and it occured both on slip planes and on twin planes.

This research was supported by funds from the Naval Air Systems Command and the Office of Naval Research.

REFERENCES

1. P. J. E. Forsyth: Proc. Roy. Soc., 1957, vol. A242, pp. 198-202.
2. A. H. Cottrell and D. Hull: Proc. Roy. Soc., 1957, vol. A242, pp. 211-213.
3. N. F. Mott: Acta Met., 1958, vol. 6, pp. 195-197.
4. W. A. Wood, S. Mck. Cousland and K. R. Sargant: Acta Met., 1963, vol. 11, pp. 643-652.
5. J. C. Grosskreutz: Phys. Stat. Sol. (b), 1971, vol. 47, pp. 11-31.; ibid, pp. 359-396.
6. V. I. Gordienko and V. S. Ivanova: Izvestiya Akademic Nauk, S.S.S.R., Otdehenic Tekhnicheskikh, 1958, No. 3, pp. 121-125.
7. M. Hempel and E. Hillnhagen: Arch. f. Eisenhuttenwes., 1962, vol. 33, pp. 567-581.
8. I. A. Oding, V. S. Ivanova and E. S. Kosyakina: Sov. Phys. Dokl., 1965, vol. 9, pp. 816-818.
9. P. G. Partridge: Phil. Mag., 1965, vol. 12, pp. 1043-1054. P. G. Partridge and C. J. Peel: The Science, Technology and Application of Titanium, R. I. Jaffee and N. E. Promisel, eds., pp. 517-534, Pergamon Press, London, 1970.
10. M. Shimura, Y. Shinohara and Y. Takeuchi: J. Japan Inst. Metals, 1968, vol. 32, pp. 554-559.
11. M. Shimura and Y. Shinohara: ibid, pp. 559-565.
12. M. Shimura, Y. Shinohara and O. Izumi: ibid, 1969, vol. 33, pp. 391-396.
13. R. Stevenson and J. F. Breedis: Acta Met., 1975, vol. 23, pp. 1419-1429.

14. A. Akhtar and E. Teghtsoonian: Met. Trans. A, 1975, vol. 6A, pp. 2201-2208.

15. P. G. Partridge: Met. Rev., 1967, No. 118, pp. 169-194.

16. N. G. Turner and W. T. Roberts: Trans. TMS-AIME, 1968, vol. 242, pp. 1223-1230.

17. D. E. MacDonald and W. A. Wood: J. Inst. Metals 1972, Vol. 100, pp. 73.

18. J. I. Dickson, J. Ducher and A. Plumtree: Met. Trans. A, 1976, vol. 7A, pp. 1559-1565.

19. M. Sugano and C. M. Gilmore: Met. Trans. A, 1979, Vol. 10A, pp. 1400-1401.

20. O. Johari and G. Thomas: The Stereographic Projection and Its Applications, p. 68, John Wiley and Sons, Inc., New York, 1969.

21. A. S. Tetelman and A. J. McEvily, Jr.: Fracture of Structural Materials, p. 553. John Wiley and Sons, Inc., New York, 1967.

22. C. J. Beevers and M. D. Halliday: Metal Science J., 1969, Vol. 3, pp. 74-79.

23.a) Z. Nishiyama, M. Oka and H. Nakagawa: J. Japan Inst. Metals, 1965, vol. 29, pp. 133-138.; b) ibid, pp. 139-143.

24. W. G. Burgers: Physica, 1934, vol. 1, pp. 561-586.

25. H. Conrad, K. Okasaki, V. Gadgil and M. Jon: Electron Microscopy and Strength of Materials, G. Thomas, R. M. Fulrath and R. M. Fisher, Eds., pp. 438-469, University of California Press, Berkeley, 1972.

26. J. P. Owens, P. Watson and A. Plumtree: Mechanical Behavior of Materials, vol. II. - Fatigue of Metals. pp. 131- 42. Society of Materials Science, Kyoto, Japan, 1972.

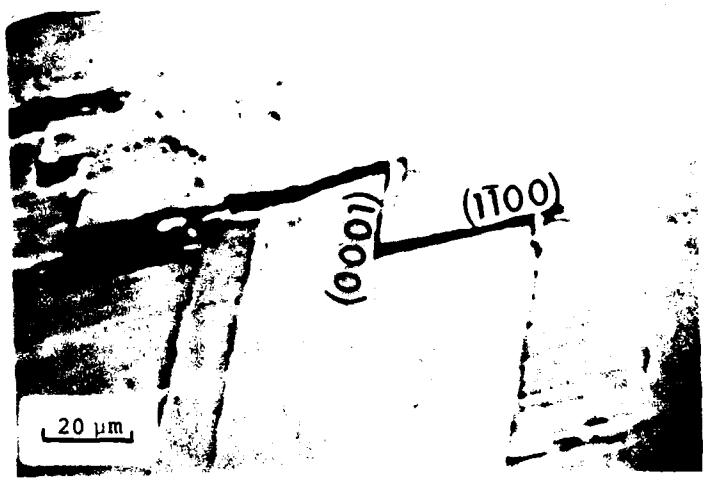

Figure 1. Fatigue microcracking observed in the vicinity of a macroscopic crack. Cyclic shear strain amplitude ±0.008.

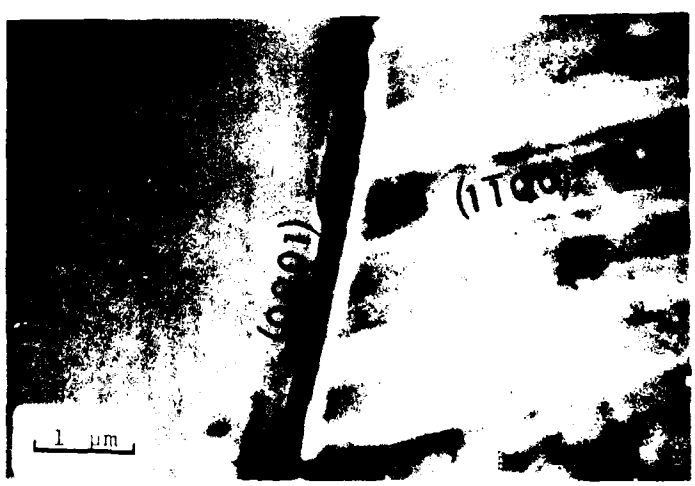

Figure 2. Cracking along a (0001) slip plane that also appears to be a subgrain boundary. Cyclic shear strain amplitude ±0.008.

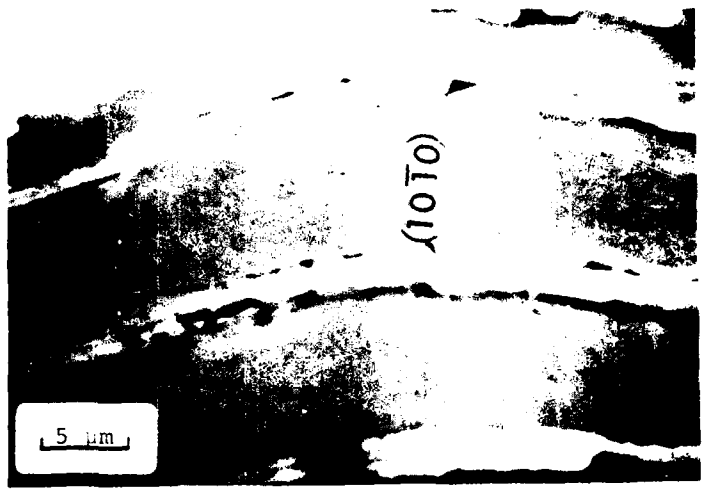

Figure 3. Slip band cracking on the (1$\bar{1}$00) and shear cracking on the (10$\bar{1}$0). Cyclic shear strain amplitude ±0.008.

Figure 4. Severe deformation surrounding a tensile mode crack propagating on a (11$\bar{2}$0) plane after cycling at ±0.008 cyclic shear strain amplitude.

Figure 5. Localized shear microcracking on slip and twin planes along a macroscopic tensile fatigue crack after cycling at ±0.003.

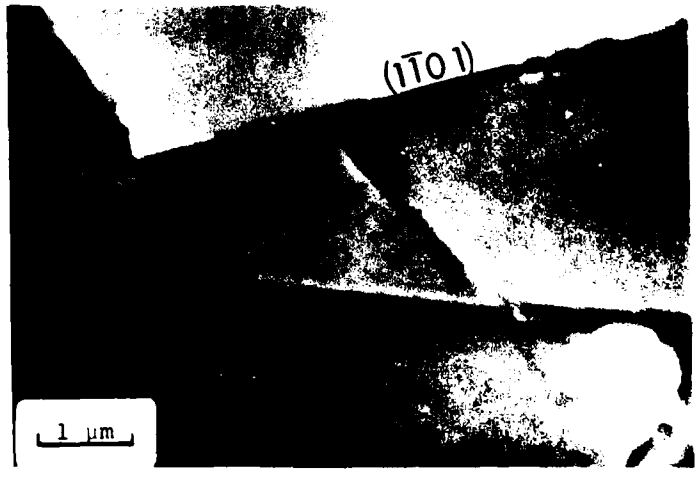

Figure 6. Localized fatigue cracking on the twin planes (11$\bar{2}$3) and {11$\bar{0}$1} after cycling at ±0.003.

Figure 7. Localized fatigue cracking on a $(\bar{1}102)$ twin plane after cycling at ±0.003.

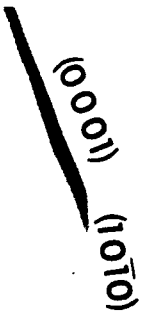

0.5 μm

Figure 8. The tip of a fatigue crack changing from a (0001) plane to a $(10\bar{1}0)$ plane. No slip lines were observed at the crack tip. Cyclic shear strain amplitude ±0.003.

Corrosion and Corrosion-Fatigue Behavior of Ti-4.5Aℓ-5Mo-1.5Cr (Corona 5) and Ti-6Aℓ-4V

M. Ashraf Imam*, Anna C. Fraker**, Karen M. Speck** and Charles M. Gilmore*

*School of Engineering and Applied Science
The George Washington University, Washington, DC 20052, USA
**Metal Science and Standards Division
The National Bureau of Standards, Washington, DC 20052, USA

ABSTRACT

The electrochemical, corrosion-fatigue and microstructure properties of the alloy Ti-4.5Aℓ-5Mo-1.5Cr (Corona 5) were determined. These properties of Corona 5 are compared, where possible, with the as received properties of the alloy Ti-6Aℓ-4V. The microstructure of Corona 5 which was beta processed with the finishing temperature below the beta transus, consists of large α-Ti grains in a matrix of β-Ti laths and needles and β-Ti. The microstructure of Ti-6Aℓ-4V which was mill annealed at 760°C for two hours, consists of large α-Ti grains with some grain boundary β-Ti.

Corrosion-fatigue tests were conducted in Hanks' buffered saline solution at a temperature of 37°C and solution pH of 7.4. Specimens were subjected to fully reversed torsion fatigue in a flowing solution with a frequency of 1Hz for the sinusoidal loading. The electrode potential was monitored to follow the corrosion-fatigue process. At lower strain levels, the Corona 5 alloy has a longer corrosion-fatigue life than the alloy Ti-6Aℓ-4V while the opposite is true for higher strains. The open-circuit electrode potential of each alloy reached a steady value with the metal in saline solution at 37°C, except at a shear strain of ±0.01 for Corona 5 where a potential drop to more negative values occured just before failure of the specimen. This potential becomes more electronegative at the onset of the applied cyclic strain. The electrode potential drop increases with increased strain. The potentiostatic polarization measurements were made in Hanks' saline solution

by applying a positive voltage at a rate of 6mv per minute and the solution had a pH of 7.4 and was held at a temperature of 37°C. The anodic polarization behavior shows that Corona 5 is slightly less corrosion resistance that Ti-6Al-4V below the breakdown potential but more corrosion resistant above the breakdown potential.

LIST OF TABLES

Table I. Chemical composition of Corona 5 and Ti-6Al-4V alloys in weight percent.

Table II. Hanks' solution.

Table III. Corrosion-fatigue life of Corona 5 and Ti-6Al-4V in Hanks' solution at 37°C.

LIST OF FIGURE CAPTIONS

Figure 1. Configuration of 24 x 5 x 3 inch block and orientation of specimens.

Figure 2. Test cell for the corrosion-fatique experiment.

Figure 3. Perspective view of a cube of Corona 5 in the as received condition showing α-Ti grains in a matrix of α-Ti laths and β-Ti 500x.

Figure 4. Transmission electron micrograph of Corona 5 in the as received condition showing α-Ti grains in a matrix of α-Ti laths and needles and β-Ti.

Figure 5. Light micrograph of Ti-6Al-4V in the as received condition showing α-Ti and β-Ti.

Figure 6. Transmission electron micrograph of Ti-6Al-4V in the as received condition showing α-Ti and β-Ti.

Figure 7. Open circuit potential Vs. time curve for Corona 5 as indicated during corrosion-fatigue testing with a shear strain $\gamma = \pm 0.0187$ in Hanks' solution (pH = 7.4) at 37°C.

Figure 8. Open circuit potential Vs. time curve for Corona 5 as indicated during corrosion-fatigue testing with a shear strain $\gamma = \pm 0.01$ in Hanks' solution (pH = 7.4) at 37°C.

Figure 9. Open circuit potential Vs. time curves for Ti-6Al-4V as indicated during corrosion-fatigue testing with a shear strain $\gamma = \pm 0.0187$ in Hanks' solution (pH = 7.4) at 37°C.

Figure 10. Open circuit potential Vs. time curves for Ti-6Al-4V as indicated during corrosion-fatigue testing with a shear strain $\gamma = \pm 0.01$ in Hanks' solution (pH = 7.4) at 37°C.

Figure 11. Anodic polarization curves for Corona 5 and Ti-6Al-4V.

CORROSION AND CORROSION-FATIGUE BEHAVIOR OF Ti-4.5Al-5Mo-1.5Cr (Corona 5) and Ti-6Al-4V

INTRODUCTION

The titanium alloy, Ti-4.5Al-5Mo-1.5Cr (Corona 5), was developed to obtain a material with improved fracture toughness over the widely used alloy, Ti-6Al-4V. Like Ti-6Al-4V, this alloy also is heat treatable and can be used as a high strength material. Since this is a relatively new alloy, much data is needed concerning its properties and durability in service. One of the problem areas which needs to be investigated is that of corrosion-fatigue since metal and alloy failures in aqueous environments can be due to this process. Corrosion is an electrochemical reaction of the metal with the environment, while fatigue is a mechanical process which occurs under repeated loading. One of the more interesting aspects of corrosion-fatigue is that both elements (corrosion and fatigue) contribute to the process, acting jointly to produce a result that is more severe than either of these two elements acting alone. Thus, the processes are complimentary; corrosion accelerates fatigue and fatigue accelerates corrosion.

This paper deals with the electrochemical, corrosion-fatigue and microstructural properties of the alloy Ti-4.5Al-5Mo-1.5Cr (Corona 5) and compares, where possible, the properties of Corona 5 with Ti-6Al-4V. Both alloys are of the alpha-beta type, are heat treatable, and exhibit mechanical properties which are strongly influenced by microstructural changes. The alloy Ti-6Al-4V has been investigated more extensively and some of its corrosion-fatigue properties have been reported previously.[1] The newer alloy, Corona 5 is richer in beta stabilizers having a beta transus temperature about 55°C lower, and a higher fracture toughness at higher strength levels than the Ti-6Al-4V alloy.[2]

EXPERIMENTAL PROCEDURE

Specimens of Corona 5 were prepared from three inch thick plate as shown in Figure 1 with chemical composition given in Table I. Corrosion-fatigue tests specimens were cut along the rolling direction and machined to a cylindrical form with a 0.65-cm diameter and a 7.6-cm length. A 1.27-cm section in the center was machined to a diameter of 0.50 cm. This center section, which was to be exposed to the solution, was mechanically polished through a 0.05-μm alumina polishing powder to produce a smooth, scratch-free surface. Specimens were washed with cotton in water and alcohol and ultrasonically cleaned in ethyl alcohol to remove any residual polishing material. This was followed by steam sterilization at 120°C and 0.10 MPa.

The environmental test cell for the corrosion-fatigue test is shown in Figure 2. This cell was placed on the fatigue machine and tubes were connected to a pump which circulated the saline solution from a reservoir. The saline solution was Hanks' solution and the description for mixing stock for 20 liters of this solution is given in Table II. This is a buffered solution with a pH of 7.4. These solutions were maintained at a temperature of 37°C throughout the test. The electrode potential of the specimen was measured versus a standard calomel electrode and was monitored with a strip chart recorder. Fatigue tests were conducted with an R value of -1 at shear strain of ±0.01 and ±0.187 with a frequency of 1Hz for the sinusoidal loading.

Microstructural analyses were conducted using methods of light microscopy, transmission and scanning electron microscopy and electron diffraction. Specimens for optical observation were mechanically polished through 0.05-μm alumina polishing powder and etched by swabbing in a solution 50% lactic acid, 33% nitric acid and 17% hydrofluoric acid, and then by

immersing in Kroll's reagent (3.5% HNo_3, 1.5% HF and 95% H_2o) for 5 to 10 seconds. Thin foils for TEM were produced by electropolishing sections of the material which were cut from the bulk material by Spark discharge cutting. The electropolishing was done in a solution 62.5% methanol, 31% butanol and 6.5% of 70% perchloric acid at 13.9 volt and -40 to -50°C.

Specimens for corrosion tests were cut in 2 mm. thick sections of 1.5 cm x 2 cm in size and were mechanically polished through a 0.05 m alumina polishing powder to produce a scratch-free surface. Individual specimens were spot welded to a wire lead and the surface was repolished with 0.05 m alumina to remove any film which would have formed in the welding process. The specimen was mounted into a glass rod with epoxy. Then the epoxy and a large portion of the specimen were covered with an insulating microstop leaving a given specimen area exposed to the test solution. The specimen area usually fell within the range of 0.5 cm^2 to 0.8 cm^2. This specimen (anode) faced a counter electrode (cathode) which had a surface area six or eight times greater than the specimen. Potentiostatic anodic polarization measurements were made from open circuit potential in the noble direction until the breakdown potential of the given material was reached. The potential was increased at a rate of .006V/min. Electrode potentials were measured versus a saturated calomel electrode. The solution used in these tests was Hanks' solution. This is a buffered solution with a pH of 7.4. The pH can be altered by adding an acid or an alkali. These solutions were maintained at a temperature of 37°C throughout the tests.

RESULTS AND DISCUSSION

Microstructure

Light and transmission electron micrographs representative of Corona 5 are shown in Figures 3 and 4, respectively. The microstructure consists of large α-Ti grains in a matrix of α-Ti laths and needles and β-Ti. This material has gone under primary processing at 1900°F, secondary processing at 1800°F and rolling with finish temperature of 1500°F. This microstructure of this material could be changed to produce a higher corrosion fatigue resistance and this work is in progress.[3] For comparative study the light and transmission electron micrographs of mill annealed Ti-6Al-4V alloy are shown in Figures 5 and 6. The mill annealed Ti-6Al-4V alloy has a microstructure consisting of large α-Ti grains with some grain boundary β-Ti. Selected area electron diffraction was used in the microstructural analysis.

Microscopic observation of the fractured surfaces of Corona 5 and Ti-6Al-4V specimens showed multiple crack initiation sites. A given fracture had both transverse and longitudinal breakage. Many cracks, parallel to the specimen axis, were present and they ran the entire length of the specimen.

Mechanical Tests

The results of the corrosion-fatigue tests at shear strains of ± 0.010 and ± 0.0187 are presented in Table III. The results indicate that at lower strain levels, the Corona 5 alloy has a longer corrosion fatigue life than Ti-6Al-4V while the opposite is true for higher strains.

Electrochemical Measurements

Coupled with the mechanical action of fatigue in these tests was the

corrosive environment. Some attempt was made to gain information relating to the formation of protective films on the metal in the solution and the cracking of the oxide film and the metal specimen. The measurement of the open circuit electrode potential of a metal specimen can give an indication of the formation or breakdown of the surface oxide film. If the electrode potential vs. time rises in the positive direction, the indication is that a protective surface oxide film is forming. If the electrode potential rises and levels off, the surface oxide film has formed and remains intact. If the electrode potential is erratic, the surface film is unstable and probably pitting is occuring. Dropping of the electrode potential in the negative direction indicates dissolution of film, cracking of the film or other film breakdown which leads to corrosion. The open circuit potential vs. time curves for Corona 5 and Ti-6Al-4V during corrosion fatigue testing are shown in Figures 7 through 10. When the fatigue is started the electrode potential drops as shown in Figures 7 through 10. The magnitude of this drop in potential is dependent on the applied load of the fatigue test. This potential drop indicates cracks in the oxide film. The orientation of these cracks is related to the metal microstructure and the fatigue deformation. As the test progresses, some of these cracks become passivated with an oxide film again while other cracks remain exposed to the solution and as a result of the environmental and the mechanical action are subject to propagation. The repassivation of some of the cracks under the environmental and mechanical conditions of the test could account for the positive rise in the potential time curve and the leveling off of this curve. After failure, the electrode potential goes in the positive direction and in the absence of fatigue, a surface film again covers the metal.

The general differences in electrode potential versus time curves for Corona 5 and Ti-6Aℓ-4V with shear strain ±0.0187 are shown in Figures 7 and 9. Shortly after the initiation of fatigue, there is an arrest in the electrode potential for the Corona 5 and as time and fatigue progress, the potential drop, rises slightly and levels off at a value more negative than the mill annealed Ti-6Aℓ-4V. The maximum drop in potential of Corona 5 was -0.94 versus SCE whereas for Ti-6Aℓ-4V was -1.1v versus SCE. The electrode potential versus time curves for Corona 5 and Ti-6Aℓ-4V with shear strain ±0.010 are shown in Figures 8 and 10. The trend of the two curves is similar as fatigue progresses except closed to the failure of the specimen where potential for Corona 5 drops to a more negative value.

The anodic polarization behavior of the two alloys in Hanks' physiological saline solution is shown in Figure 11. The potentiostatic polarization measurements were made by applying a positive voltage at a rate of 6mv per minute and the solution had a pH of 7.4 and was held at a temperature of 37°C. These anodic polarization curves permit a comparison of the passive regions of the two materials and also their breakdown potentials. The breakdown potential is indicated by an increase in the current density and occurs at 2.0 volts for Ti-6Aℓ-4V and at 2.4 volts for Corona 5. The Corona 5 has a slightly higher current density but it has a higher breakdown potential. This implies that Corona 5 is slightly less corrosion resistant than Ti-6Aℓ-4V below the breakdown potential Ti-6Aℓ-4V, but the breakdown potential of Ti-6Aℓ-4V is lower than Corona 5 and once this potential of 2 volts is surpassed the Corona 5 is more corrosion resistant.

CONCLUSIONS

It can be concluded from this study that at lower strain levels, the Corona 5 alloy has a longer corrosion-fatigue life than the mill annealed Ti-6Aℓ-4V while the opposite is true for higher strains. The open circuit electrode potential of the alloys reached a steady value for a given metal in saline solution at 37°C except at shear strain of ±0.01 for Corona 5 where a potential drop to more negative values occured just before failure of the specimen. The potential becomes more electronegative at the onset of the applied cyclic strain and the electrode potential drop increases with increased strain. The anodic polarization behavior shows that Corona 5 is slightly less corrosion resistant than Ti-6Aℓ-4V below the breakdown potential while the Corona 5 is more corrosion resistant above the breakdown potential.

TABLE I

Chemical composition of Corona 5 and Ti-6Aℓ-4V alloys in weight percent.

a. Corona 5 (24 x 5 x 3 inch block was obtained as beta processed with finishing temperature below the beta transus).

Aℓ	Mo	Cr	O	N_2	Fe	H_2	C	Ti
4.4	5.1	1.46	0.183	0.011	0.20	0.0018	0.065	Base

b. Ti-6Aℓ-4V (1/4 inch diameter rod was mill annealed at 1400°F for two hours).

Aℓ	V	Fe	C	O	N	H	Ti
6.20	4.05	0.15	0.013	0.13	0.011	0.0058	Base

TABLE II

Hanks' Solution

SOLUTION A:	160 g NaCl 8 g KCl 4 g $MgSO_4.7H_2O$ in 800 ml H_2O
SOLUTION B:	2.8 g $CaCl_2$ in 100 ml H_2O
SOLUTION C:	A + B + 100 ml H_2O + 2 ml $CHCl_3$ (chloroform)
SOLUTION D:	1.2 g $Na_2HPO_4.7H_2O$ 2.0 g $NaH_2PO_4.H_2O$ 20.0 g glucose 2.0 ml $CHCl_3$ in 800 ml H_2O - diluted to 1000 ml
SOLUTION E:	1.4% $NaHCO_3$ = 7 g $NaHCO_3$ in 500 ml H_2O
FINAL SOLUTION:	50 ml C 50 ml D 24 ml E 900 ml H_2O few drops chloroform

TABLE III

Corrosion-Fatigue Life of Corona 5 and Ti-6Aℓ-4V in Hanks' Solution at 37°C

Applied Shear Strain	Material	Cycles to Failure
±0.010	Corona 5	6.5×10^5 (1)
	Ti-6Aℓ-4V	2.2×10^5 (2)
±0.0187	Corona 5	1.8×10^4 (1)
	Ti-6Aℓ-4V	3.5×10^4 (2)

1. 2 specimens tested
2. 4 specimens tested

REFERENCES

1. Imam, M. A., Gilmore, C. M. and Fraker, A. C., Proc. Conf. Environ. Degrad. Eng. Matls., M. R. Louthan, Jr. and R. P. McNitt, Eds., Virginia Polytech. Inst., Blacksburg, VA, 1977, pp. 783-790.

2. Berryman, R. G., Chesnutt, J. C. and Froes, F. H., Metal Progress, Dec. 1977, p. 40.

3. Imam, M. A., D.Sc. Thesis, George Washington University, Washington D.C., 1978.

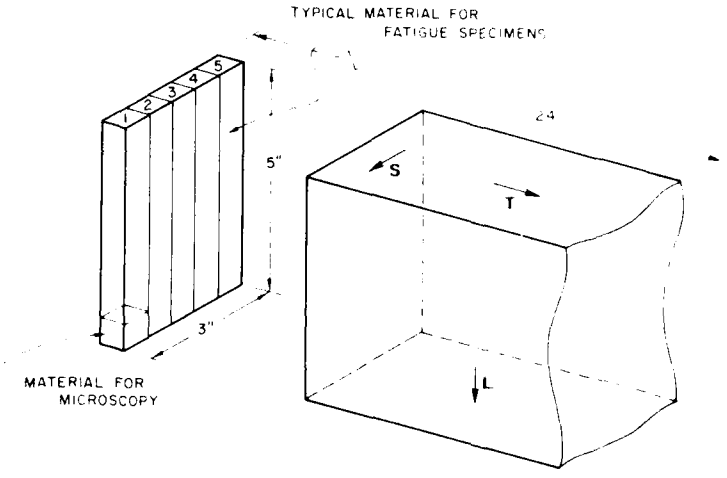

Figure 1. Configuration of 24 x 5 x 3 inch block and orientation of specimens.

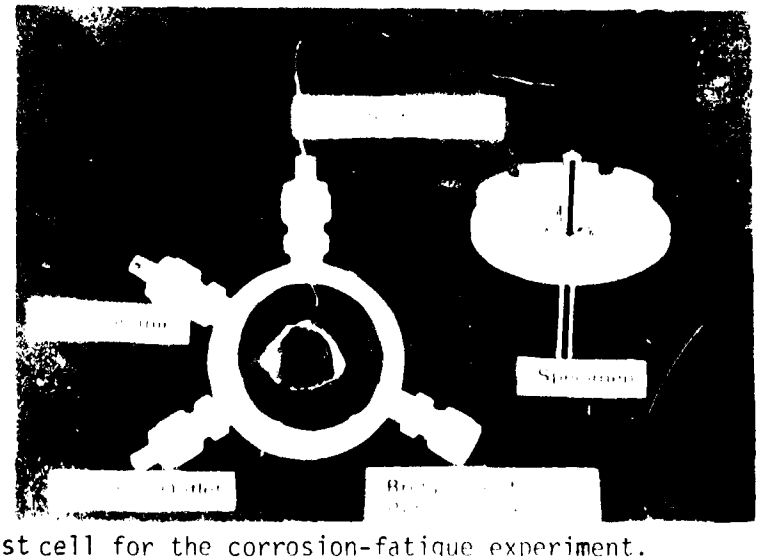

Figure 2. Test cell for the corrosion-fatigue experiment.

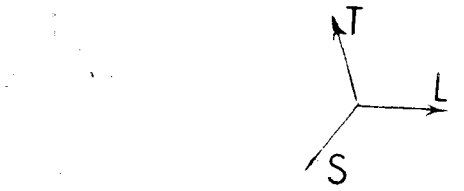

Figure 3. [illegible] in the as received condition [illegible] laths and --Ti. 500x.

Figure 4. Tr[illegible] [illegible] zone 5 in the as received condition [illegible] array of --Ti laths and [illegible]

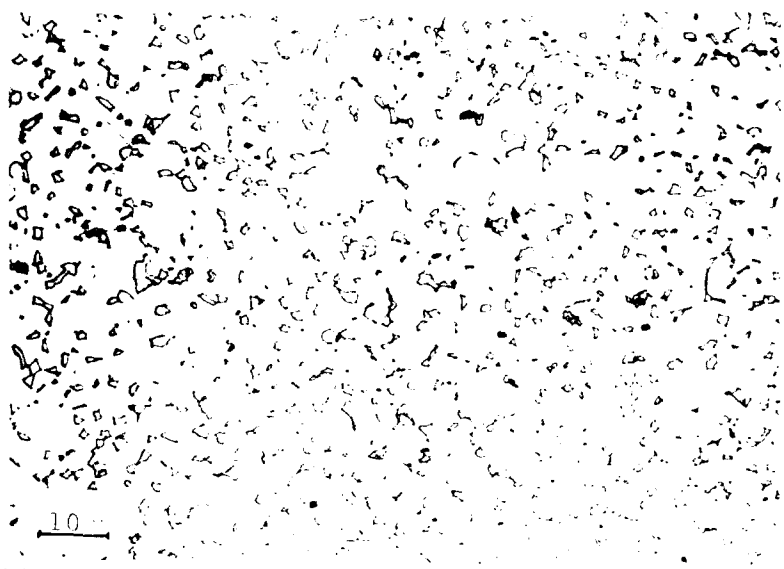

Figure 5. Light micrograph of Ti-6Al-4V in the as received condition showing α-Ti and β-Ti.

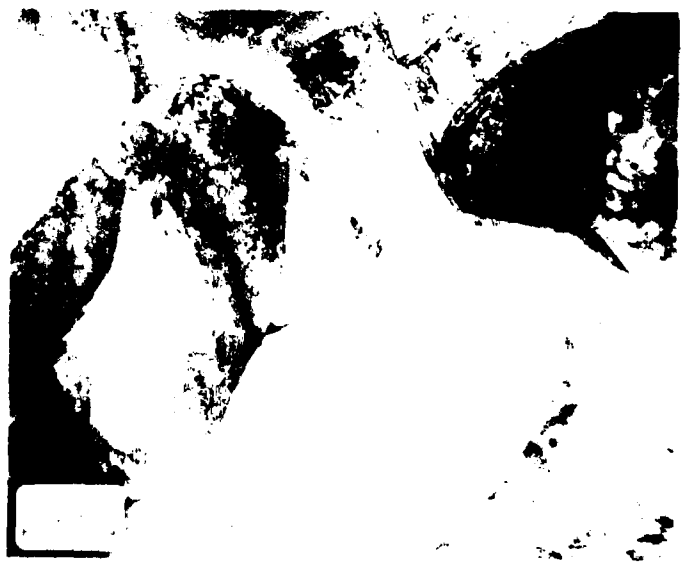

Figure 6. Transmission electron micrograph of Ti-6Al-4V in the as received condition showing α-Ti and β-Ti.

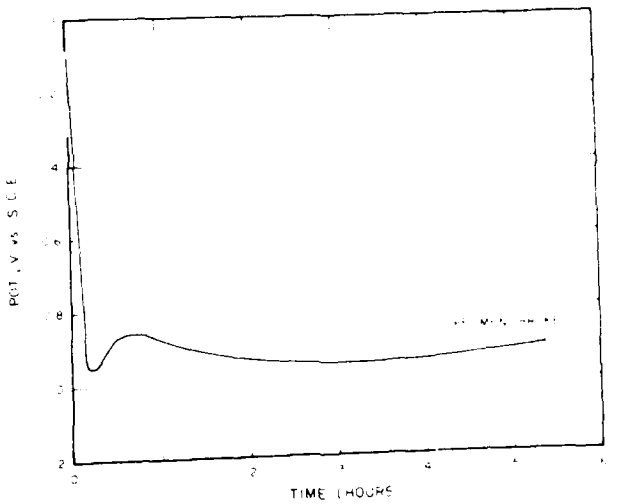

Figure 7. Open circuit potential Vs. time curve for Corona 5 as indicated during corrosion-fatigue testing with a shear strain $\gamma = 0.0187$ in Hanks' solution (pH = 7.4) at 37°C.

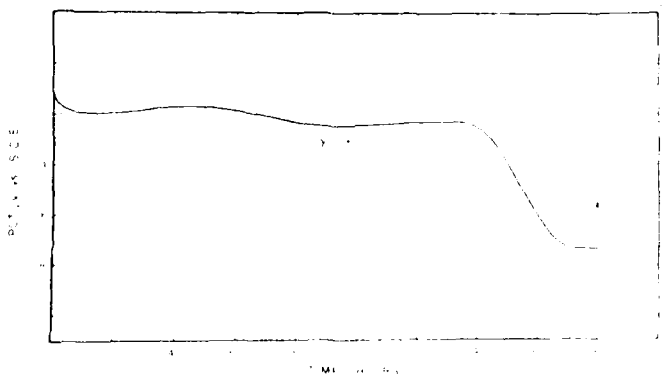

Figure 8. Open circuit potential Vs. time curve for Corona during corrosion-fatigue testing with a shear Hanks' solution (pH = 7.4) at 37°C.

AD-A094 197 GEORGE WASHINGTON UNIV WASHINGTON D C SCHOOL OF ENGI--ETC F/G 11/6
FATIGUE AND MICROSTRUCTURAL PROPERTIES OF QUENCHED TI-6AL-4V, A--ETC(U)
SEP 80 C M GILMORE, M A IMAM, M SUGANO N00019-78-C-0269
UNCLASSIFIED TR-5 NL

2 OF 2
AD A094197

END
DATE FILMED
2-81
DTIC

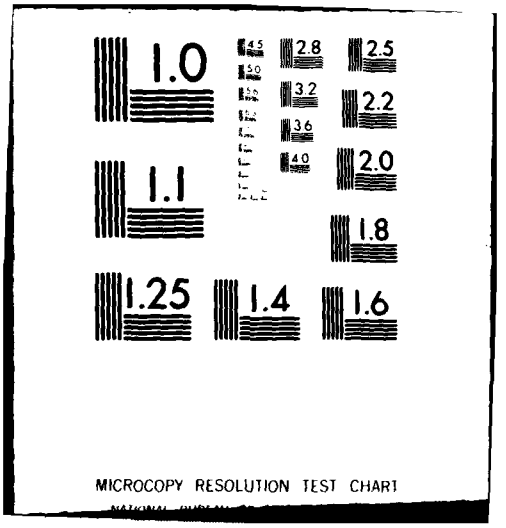
1.0
1.1
1.25
1.4
1.6
1.8
2.0
2.2
2.5
2.8
3.2
3.6
4.0
4.5
5.0
MICROCOPY RESOLUTION TEST CHART

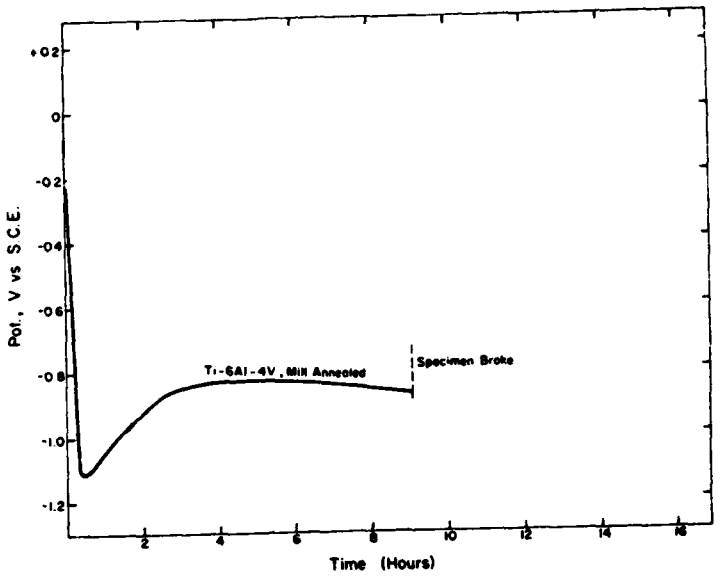

Figure 9. Open circuit potential Vs. time curves for Ti-6Aℓ-4V as indicated during corrosion-fatigue testing with a shear strain $\gamma=\pm 0.0187$ in Hanks' solution (pH = 7.4) at 37°C.

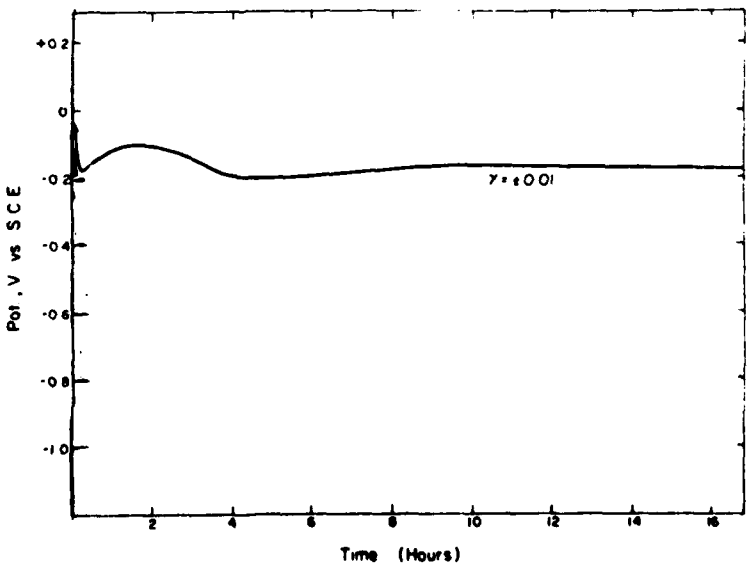

Figure 10. Open circuit potential vs. time curves for Ti-6Aℓ-4V as indicated during corrosion-fatigue testing with a shear strain $\gamma=\pm 0.01$ in Hanks' solution (pH = 7.4) at 37°C.

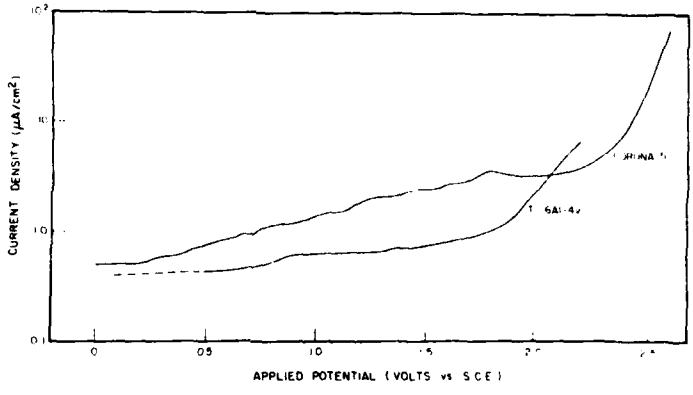

Figure 11. Anodic polarization curves for Corona 5 and Ti-6Aℓ-4V.

SECURITY CLASSIFICATION OF THIS PAGE (When Data Entered)

REPORT DOCUMENTATION PAGE		READ INSTRUCTIONS BEFORE COMPLETING FORM
1. REPORT NUMBER	2. GOVT ACCESSION NO. AD-A094 197	3. RECIPIENT'S CATALOG NUMBER
4. TITLE (and Subtitle) A) FATIGUE AND MICROSTRUCTURAL PROPERTIES OF QUENCHED Ti-6Al-4V B) A CRYSTALLOGRAPHIC STUDY OF FATIGUE DAMAGE IN TITANIUM. C) CORROSION & CORROSION FATIGUE BEHAVIOR OF Ti-4.5Al-5Mo-1.5Cr & Ti-6Al-4V		5. TYPE OF REPORT & PERIOD COVERED FINAL
		6. PERFORMING ORG. REPORT NUMBER V
7. AUTHOR(s) A) M. A. IMAM and C. M. GILMORE B) M. SUGANO AND C. M. GILMORE C) M. A. IMAM, A. C. FRAKER, K. M. SPECK & C. M. GILMORE		8. CONTRACT OR GRANT NUMBER(s) N00019-78-C-0269
9. PERFORMING ORGANIZATION NAME AND ADDRESS SCHOOL OF ENGINEERING AND APPLIED SCIENCE THE GEORGE WASHINGTON UNIVERSITY WASHINGTON, D.C. 20052		10. PROGRAM ELEMENT, PROJECT, TASK AREA & WORK UNIT NUMBERS
11. CONTROLLING OFFICE NAME AND ADDRESS NAVAL AIR SYSTEMS COMMAND WASHINGTON, D.C. 20361		12. REPORT DATE September 1980
		13. NUMBER OF PAGES 100
14. MONITORING AGENCY NAME & ADDRESS(if different from Controlling Office)		15. SECURITY CLASS. (of this report) UNCLASSIFIED
		15a. DECLASSIFICATION/DOWNGRADING SCHEDULE

16. DISTRIBUTION STATEMENT (of this Report)

APPROVED FOR PUBLIC RELEASE; DISTRIBUTION UNLIMITED

17. DISTRIBUTION STATEMENT (of the abstract entered in Block 20, if different from Report)

18. SUPPLEMENTARY NOTES

19. KEY WORDS (Continue on reverse side if necessary and identify by block number)

TITANIUM ALLOYS, Ti-6Al-4V, MARTENSITE, RETAINED BETA, FATIGUE, STRAIN INDUCED MARTENSITE TRANSFORMATION, CRYSTALLOGRAPHY, SLIP PLANES, CRACK INITIATION, CRACK PROPAGATION, CORONA 5, CORROSION, CORROSION-FATIGUE ELECTROCHEMICAL POTENTIAL.

20. ABSTRACT (Continue on reverse side if necessary and identify by block number)

A. FATIGUE AND MICROSTRUCTURAL PROPERTIES OF QUENCHED Ti-6Al-4V: THE MECHANICAL PROPERTIES AND MICROSTRUCTURES OF Ti-6Al-4V WERE DETERMINED FOR SPECIMENS HEAT TREATED AT TEMPERATURES FROM 843°C TO 1065°C FOR 10 MINUTES AND WATER QUENCHED; THESE PROPERTIES WERE COMPARED WITH THOSE OF α-β ANNEALED SPECIMENS. SPECIMENS HEAT TREATED AT 900°C AND WATER QUENCHED HAD HIGHER FATIGUE LIVES BY A FACTOR OF FOUR TO TEN RELATIVE TO THE OTHER TREATMENTS, IN A.DITION THIS TREATMENT RESULTED IN HIGH DUCTILITY, YIELD STRENGTH AND ELASTIC

DD FORM 1 JAN 73 1473 EDITION OF 1 NOV 65 IS OBSOLETE
S/N 0102-014-6601

SECURITY CLASSIFICATION OF THIS PAGE (When Data Entered)

MODULUS. MICROSTRUCTURE STUDIES UTILIZING OPTICAL AND TRANSMISSION MICROSCOPY SHOWED THAT THE IMPROVED FATIGUE LIVES WERE A RESULT OF A STRAIN INDUCED TRANSFORMATION OF RETAINED β TO α′ MARTENSITE. ISOTHERMAL AGING OF AS QUENCHED SPECIMENS REDUCED THE FATIGUE LIVES AND THE RETAINED β WAS THERMALLY ACTIVATED TO TRANSFORM TO α′ MARTENSITE. THE β TO α′ MARTENSITE TRANSFORMATION OBSERVED WAS THEREFORE AN ISOTHERMAL MARTENSITE TRANSFORMATION WHEREAS IT IS PRESENTLY ASSUMED THAT THIS TRANSFORMATION IS ALWAYS athermal. THE AMOUNT OF RETAINED β AND ITS RELATIVE STABILITY WAS SHOWN TO DEPEND UPON THE HEAT TREATMENT TEMPERATURE. THE LOWER THE HEAT TREATMENT TEMPERATURE BELOW THE β TRANSUS THE SMALLER THE AMOUNT OF β PHASE PRESENT BEFORE THE QUENCH AND THE RICHER THE β PHASE IN β STABILIZER. THE GREATER THE CONCENTRATION OF β STABILIZER IN THE β PHASE THE GREATER THE PROBABILITY THAT THE β PHASE WAS RETAINED. LOW HEAT TREATMENT TEMPERATURES RESULTED IN A SMALL AMOUNT OF MORE STABLE β PHASE, AND HIGH HEAT TREATMENT TEMPERATURES RESULTED IN A GREATER AMOUNT OF β THAT WAS LESS STABLE AND WAS MORE PROBABLE TO TRANSFORM TO α′ MARTENSITE DURING A WATER QUENCH.

B. A CRYSTALLOGRAPHIC STUDY OF FATIGUE DAMAGE IN TITANIUM: LARGE-GRAIN SPECIMENS WITH AVERAGE GRAIN SIZE 0.5 IN. (12.7 mm) OF COMMERCIAL PURITY TITANIUM WERE SUBJECTED TO TORSIONAL CYCLIC STRAIN AT TWO DIFFERENT AMPLITUDES: ±0.008 AND ±0.003. FATIGUE DAMAGE WAS STUDIED BY SCANNING ELECTRON MICROSCOPY AND CRYSTAL ORIENTATIONS WERE DETERMINED BY X-RAY DIFFRACTION AND SURFACE TRACE ANALYSIS. IT WAS FOUND THAT CYCLIC STRAIN AMPLITUDE INFLUENCED THE DEFORMATION MODE AND THE NATURE OF THE MACROSCOPIC CRACK PROPAGATION. AT HIGH STRAIN AMPLITUDES THE NORMAL SLIP PROCESSES WERE OBSERVED AND MICROCRACKING WAS OBSERVED ON THE (0001), AND $\{1\bar{1}00\}$ SLIP PLANES. THE MACROSCOPIC CRACK PROPAGATION WAS DOMINATED BY THE STAGE I SHEAR MODE; HOWEVER, SOME STAGE II TENSILE MODE PROPAGATION WAS OBSERVED AFTER EXTENSIVE STAGE I PROPAGATION. AT LOW STRAIN AMPLITUDE TWIN PLANE CRACKING WAS OBSERVED ON THE $\{10\bar{1}1\}$, $\{10\bar{1}0\}$, AND $\{11\bar{2}3\}$ PLANES IN ADDITION TO NORMAL SLIP PLANE CRACKING, AND THE MACROSCOPIC CRACK PROPAGATION WAS DOMINATED BY THE STAGE II TENSILE MODE. HOWEVER, MICROSCOPIC EXAMINATION SHOWED THE MACROSCOPIC TENSILE MODE CRACKS TO BE COMPOSED OF MICROSCOPIC SHEAR MODE CRACKS ALONG SLIP PLANES AND TWIN PLANES. AT BOTH LOW AND HIGH STRAIN AMPLITUDES CRACKING WAS OBSERVED ON THE $\{11\bar{2}0\}$ PLANE WHICH IS NEITHER A SLIP OR TWIN PLANE IN TITANIUM. IT IS PROPOSED THAT THIS CRACKING MODE WAS A RESULT OF A DISLOCATION REACTION FORMING SESSILE DISLOCATIONS ON THE $\{11\bar{2}0\}$ PLANE.

C. CORROSION & CORROSION-FATIGUE BEHAVIOR OF Ti-4.5Aℓ-5Mo-1.5Cr (CORONA 5) AND Ti-6Aℓ-4V: THE ELECTROCHEMICAL, CORROSION-FATIGUE AND MICROSTRUCTURE PROPERTIES OF THE ALLOY Ti-4.5Aℓ-5Mo-1.5Cr (CORONA 5) WERE DETERMINED. THESE PROPERTIES OF CORONA 5 ARE COMPARED, WHERE POSSIBLE, WITH THE AS RECEIVED PROPERTIES OF THE ALLOY Ti-6Aℓ-4V. THE MICROSTRUCTURE OF CORONA 5 WHICH WAS BETA PROCESSED WITH THE FINISHING TEMPERATURE BELOW THE BETA TRANSUS, CONSISTS OF LARGE α-Ti GRAINS IN A MATRIX OF β-Ti LATHS AND NEEDLES AND β-Ti. THE MICROSTRUCTURE OF Ti-6Aℓ-4V WHICH WAS MILL ANNEALED AT 760°C FOR TWO HOURS, CONSISTS OF LARGE α-Ti GRAINS WITH SOME GRAIN BOUNDARY β-Ti. CORROSION-FATIGUE TESTS WERE CONDUCTED IN HANKS BUFFERED SALINE SOLUTION AT A TEMPERATURE OF 37°C AND SOLUTION pH OF 7.4. SPECIMENS WERE SUBJECTED TO FULLY REVERSED TORSION FATIGUE IN A FLOWING SOLUTION WITH A FREQUENCY OF 1Hz FOR THE SINUSOIDAL LOADING. THE ELECTRODE POTENTIAL WAS MONITORED TO FOLLOW THE CORROSION-FATIGUE PROCESS. AT LOWER STRAIN LEVELS, THE CORONA 5 ALLOY HAS A LONGER CORROSION-FATIGUE LIFE THAN THE ALLOY Ti-6Aℓ-4V WHILE THE OPPOSITE IS TRUE FOR HIGHER STRAINS. THE OPEN-CIRCUIT ELECTRODE POTENTIAL OF EACH ALLOY REACHED A STEADY VALUE WITH THE METAL IN SALINE SOLUTION AT 37°C, EXCEPT AT A SHEAR STRAIN OF ±0.01 FOR CORONA 5 WHERE A POTENTIAL DROP TO MORE NEGATIVE VALUES OCCURED JUST BEFORE FAILURE OF THE SPECIMEN. THIS POTENTIAL BECOMES MORE ELECTRONEGATIVE AT THE ONSET OF THE APPLIED CYCLIC STRAIN. THE ELECTRODE POTENTIAL DROP INCREASES WITH INCREASED STRAIN. THE POTENTIO-

STATIC POLARIZATION MEASUREMENTS WERE MADE IN HANKS' SALINE SOLUTION BY APPLYING A POSITIVE VOLTAGE AT A RATE OF 6mv PER MINUTE AND THE SOLUTION HAD A pH OF 7.4 AND WAS HELD AT A TEMPERATURE OF 37°C. THE ANODIC POLARIZATION BEHAVIOR SHOWS THAT CORONA 5 IS SLIGHTLY LESS CORROSION RESISTANCE THAT Ti-6Aℓ-4V BELOW THE BREAKDOWN POTENTIAL BUT MORE CORROSION RESISTANT ABOVE THE BREAKDOWN POTENTIAL.